

1 The spectrum of persistent volcanic flank instability: A review
2 and proposed framework based on Kīlauea, Piton de la
3 Fournaise, and Etna

4
5

6 Michael P. Poland*¹, Aline Peltier², Alessandro Bonforte³, Giuseppe Puglisi³

7

8 1 U.S. Geological Survey

9 Cascades Volcano Observatory

10 1300 SE Cardinal Ct., Suite 100

11 Vancouver, WA 98683 USA

12 Tel: +1 360-993-8906

13 mpoland@usgs.gov

14

15 2 Institut de Physique du Globe de Paris, Sorbonne Paris Cité

16 Observatoire Volcanologique du Piton de la Fournaise

17 Univ. Paris Diderot, UMR 7154 CNRS, F-97418 La plaine des Cafres, France

18

19 3 Istituto Nazionale di Geofisica e Vulcanologia

20 Sezione di Catania

21 Osservatorio Etneo, Catania 95125, Italy

22

23 * Corresponding Author

24

25

26 **USGS Disclaimer:**

27 This draft manuscript is distributed solely for purposes of scientific peer review. Its content is

28 deliberative and predecisional, so it must not be disclosed or released by reviewers. Because the

29 manuscript has not yet been approved for publication by the U.S. Geological Survey (USGS), it

30 does not represent any official USGS finding or policy.

31 **Abstract**

32 Persistent motion of the flanks of Kīlauea Volcano, Hawai‘i, has been known for several
33 decades, but has only recently been identified at other large basaltic volcanoes—namely Piton de
34 la Fournaise (La Réunion) and Etna (Sicily)—thanks to the advent of space geodetic techniques.
35 Nevertheless, understanding of long-term flank instability is based largely on the example of
36 Kīlauea, despite the large differences in the manifestations and mechanisms of the process when
37 viewed through a comparative lens. For example, the rate of flank motion at Kīlauea is several
38 times that of Etna and Piton de la Fournaise and is accommodated on a slip plane several km
39 deeper than is probably present at the other two volcanoes. Gravitational spreading also appears
40 to be the dominant driving force at Kīlauea, given the long-term steady motion of the volcano’s
41 south flank regardless of eruptive/intrusive activity, whereas magmatic activity plays a larger
42 role in flank deformation at Etna and Piton de la Fournaise. Kīlauea and Etna, however, are both
43 characterized by heavily faulted flanks, while Piton de la Fournaise shows little evidence for
44 flank faulting. A helpful means of understanding the spectrum of persistent flank motion at large
45 basaltic edifices may be through a framework defined on one hand by magmatic activity (which
46 encompasses both magma supply and edifice size), and on the other hand by the structural setting
47 of the volcano (especially the characteristics of the subvolcanic basement or subhorizontal
48 intravolcanic weak zones). A volcano’s size and magmatic activity will dictate the extent to
49 which gravitational and magmatic forces can drive motion of an unstable flank (and possibly the
50 level of faulting of that flank), while the volcano’s structural setting governs whether or not a
51 plane of weakness exists beneath or within the edifice and can facilitate flank slip. Considering
52 persistent flank instability using this conceptual structure is an alternative to using a single
53 volcano as a “type example”—especially given that the example is usually Kīlauea, which
54 defines an extreme end of the spectrum—and can provide a basis for understanding why flank
55 motion may or may not exist on other large basaltic volcanoes worldwide.

56

57 **Keywords:** flank instability; deformation; basaltic volcanism; Kīlauea; Etna; Piton de la
58 Fournaise

59

60 **1. Introduction**

61 Volcanic flank instability is clearly an important process in the evolution of large basaltic
62 volcanoes, but its manifestations and mechanisms are poorly known because insights are drawn
63 mostly from the example of Hawai‘i. This lack of depth stems from the fact that flank motion has
64 only been recognized as an important process since the mid-20th century, so opportunities for
65 study, especially outside Hawai‘i, have been limited. Indeed, space-based geodetic techniques—
66 especially Global Navigation Satellite Systems (GNSS) and Interferometric Synthetic Aperture
67 Radar (InSAR)—that evolved during the late 20th century played a key role in defining the
68 extent, rate and pattern of flank instability at many volcanoes [e.g., Owen et al, 1995; Bonforte
69 and Puglisi, 2003, González et al., 2010; Brenguier et al., 2012]. It is therefore important to ask
70 the questions of how and why flank motion varies between volcanoes, and how current
71 knowledge may be exploited to increase understanding of the process at volcanoes worldwide.

72 In 1964, James Moore, then a geologist with the U.S. Geological Survey’s Hawaiian
73 Volcano Observatory, authored two manuscripts that were the first to provide evidence of
74 instability in large basaltic volcanoes. In the first article, Moore and Krivoy [1964] proposed that
75 the south flank of Kīlauea was sliding seaward due to gravity and pressurization of the volcano’s
76 East Rift Zone, based on deformation and structures associated with eruptive activity in 1962.
77 About a decade later, the postulated seaward motion was confirmed by trilateration
78 measurements, leading subsequent authors to posit that a large earthquake might be possible due
79 to flank compression [Swanson et al., 1976]—a prescient hypothesis, since an M7.7 earthquake
80 occurred in 1975 (while the trilateration results were in press). In the second paper, Moore
81 [1964] suggested that bathymetric data from the sea floor north of the Hawaiian islands of O‘ahu
82 and Moloka‘i recorded the presence of massive landslides. This possibility was debated for
83 several decades, until comprehensive mapping of the sea floor around Hawai‘i settled the matter
84 and demonstrated beyond any doubt that massive landslides were a common process in the
85 archipelago [Moore et al., 1989].

86 In the more than half-century since Moore’s recognition of the various forms of
87 instability in Hawai‘i, flank motion and catastrophic failures have been identified at numerous
88 large basaltic volcanoes around the world. At Piton de la Fournaise (La Réunion island), for
89 example, large-scale debris avalanches have been identified offshore from marine data and have
90 been interpreted as resulting from old flank collapses [e.g. Lénat et al., 1990; Oehler et al., 2008;
91 Le Friant et al., 2011] and gravitationally driven volcanic spreading [e.g. Oehler et al., 2005;

92 Michon and Saint-Ange, 2008]. Indeed, more than 500 km³ of avalanche deposits cover the
93 eastern submarine flank of the volcano [e.g. Oehler et al., 2005]. In Sicily, the continental margin
94 off the eastern coast of Etna shows an offset due to a large bulge that is characterized by several
95 semi-circular steps, interpreted as evidence of large landslides and suggesting gravitational
96 instability of the submarine base of the edifice and extending onto the volcano's subaerial eastern
97 flank [Borgia et al., 1992; Rust and Neri, 1996; Chiocci et al., 2011; Azzaro et al., 2013].
98 Evidence for varying degrees of flank instability has also been found on many other basaltic
99 volcanoes, such as the Canary Islands [Holcomb and Searle, 1991; Urgeles et al., 1997;
100 Carracedo et al., 1999; Hürlimann et al., 2000; Krastel et al., 2001; Masson et al., 2002],
101 Galápagos [Geist et al., 2002], and Tristan de Cunha [Holcomb and Searle, 1991].

102 Flank instability is so ubiquitous that it is surprising when it is not found at a large
103 volcano, motivating investigators to ask the question “why not?” [e.g., Nakamura, 1980; Geist et
104 al., 2006]. A growing body of research is now emphasizing the importance of flank instability on
105 the evolution of large basaltic volcanoes, and also on the hazards posed by those volcanoes [e.g.,
106 Denlinger and Morgan, 2014]. Unstable flanks not only experience large earthquakes, but can
107 also fail catastrophically, resulting in large subaerial and/or submarine landslides that, for island
108 or coastal volcanoes, can trigger tsunamis. In addition, flank instability and eruptive activity feed
109 off one another. Flank motion can promote eruptive activity, repeated rift zone intrusions and
110 pressurization of a magmatic system have the ability to “push” a flank closer to some sort of
111 failure, and eruptive activity results in gravitational loading and oversteepening.

112 Despite the widespread nature of flank instability on large basaltic volcanoes, the
113 mechanisms and manifestations of the process are diverse; therefore, it would be a mistake to
114 universally apply models developed at any specific volcano. For example, Hawai‘i, despite being
115 the type locality for instability of large basaltic volcanoes, is a poor analog for the Galápagos in
116 terms of flank behavior [e.g., Poland, 2014a]. In an effort to better define the spectrum of flank
117 instability at large basaltic edifices, we review the process at three well-studied but vastly
118 different volcanoes: Kīlauea, Piton de la Fournaise, and Etna (Fig. 1). We chose these sites
119 because they are among the best-monitored and most active volcanoes in the world, and also
120 because they represent extremes across the spectrum of basaltic volcanism in terms of their sizes
121 and tectonic settings. As such, these three volcanoes provide excellent examples upon which to
122 define a conceptual framework for flank processes.

123 Here, we focus on ongoing, deep-seated, persistent flank motion (sometimes referred to
124 as “volcanic spreading” [Borgia et al., 1992; Merle and Borgia, 1996]) that can be characterized
125 by geological study and geophysical techniques. We do not explore other styles of flank motion,
126 including large-scale catastrophic collapse, which has never been witnessed and thus remains a
127 poorly understood process [e.g., Iverson, 1995]; shallow motion of surficial deposits, which may
128 be correlated with magmatic activity, as at Stromboli, Italy [Di Traglia et al., 2014]; nor transient
129 co-eruptive motion that may be associated with sector collapse at arc volcanoes, as exemplified
130 by the May 2010 deformation observed at Pacaya, Guatemala [Schaefer et al., 2015, 2016].
131 Through a comparative analysis of Kīlauea, Piton de la Fournaise, and Etna—three volcanoes
132 commonly used as type examples for large basaltic edifices [e.g., Michon et al., 2015; Peltier et
133 al., 2015a]—we find that the style and magnitude of long-term persistent instability scale with
134 the size of the host volcanic system and the character of the volcanic substrate. This general
135 framework may be useful for better understanding flank instability at other large basaltic
136 volcanoes that are not as well characterized as these three sites.

137

138 **2. Geological characteristics and eruptive activity of example volcanoes**

139 ***2.1 Kīlauea***

140 Kīlauea is the youngest and currently the most active volcano on the Island of Hawai‘i,
141 located in the middle of the Pacific Plate at the leading edge of a ~6000-km-long chain of islands
142 and seamounts that marks the activity of the Hawaiian hot spot over the past 70 million years
143 [Clague and Dalrymple, 1987; Tilling and Dvorak, 1993; Clague and Sherrod, 2014]. Given that
144 the volcano overlaps significantly with its much larger neighbor, Mauna Loa, Kīlauea’s volume
145 is difficult to determine, having been variously estimated to range between 31,600 km³
146 [Robinson and Eakins, 2006] and 11,000 km³ (Table 1) [Lipman and Calvert, 2013]. The
147 inception age of Kīlauea is probably no earlier than 275 ka, although the vigorous shield-
148 building tholeiitic stage of volcanism probably did not begin until about 100 ka [Lipman and
149 Calvert, 2013]. Magma supply to the volcano since the 1950s appears to have averaged
150 approximately 0.1 km³/yr as estimated from rates of magma storage and eruption, although
151 geophysical and geochemical monitoring data from the 2000s have documented both a surge and
152 a lull, suggesting that years-long variations in supply can and do occur [Poland et al., 2012;
153 Poland, 2014b; Anderson and Poland, 2016]. Variability in magma supply over centuries has

154 also been proposed as an explanation for cycles of effusive and explosive volcanism at Kīlauea
155 [Swanson et al., 2014].

156 Structurally, Kīlauea can be broadly described as hosting a summit caldera and two rift
157 zones (Fig. 2). The summit caldera is ephemeral, experiencing cycles of formation and filling
158 over the past several thousand years that may be tied to variations in magma supply over time
159 [Swanson et al., 2014]. Geophysical data currently support the presence of at least two magma
160 storage areas beneath Kīlauea’s summit—one at ~1.5 km beneath the center of the caldera, and a
161 second (the primary magma storage area for the volcano) about 3 km beneath the south part of
162 the caldera [e.g., Poland et al., 2014]. Kīlauea’s two rift zones radiate away from the summit to
163 the east and southwest. There is some evidence that each rift zone is actually comprised of two
164 parts at different depths that connect to the shallower and deeper summit magma storage areas
165 [Poland et al., 2014]. The rift systems provide a means for lateral magma transport from the
166 summit to the distal flanks of the volcano, where magma may be stored in small reservoirs
167 within the rift zone or erupted at the surface. The deep rift zones, below about 3 km depth, show
168 evidence of steady opening [Delaney et al., 1990; Owen et al., 1995, 2000a], perhaps driven by
169 the presence of dense cumulates [Clague and Denlinger, 1994].

170 In addition to the caldera and rift zones, Kīlauea hosts two normal fault systems, both of
171 which trend ENE-WSW (the dominant structural grain of the volcano; Fig.2) [Johnson et al.,
172 2015]. The Koa‘e Fault System, comprised of mostly north-facing normal faults, links the East
173 and Southwest Rift Zones south of the caldera and has been a site of occasional magmatic
174 intrusions [Swanson et al., in prep]. The Hilina Fault System is made up of south-facing normal
175 faults along the volcano’s southern coast and is associated with instability of that flank [Cannon
176 and Bürgmann, 2001; Cannon et al., 2001; Denlinger and Morgan, 2014], having last ruptured
177 during the 1975 M7.7 Kalapana earthquake [Lipman et al., 1985].

178 Eruptive activity at Kīlauea alternates between centuries-long periods of lava effusion
179 and centuries-long periods of explosive eruptions [Swanson et al., 2014]. Since the early 1800s,
180 eruptions have been mostly effusive from the summit and both rift zones. East Rift Zone eruptive
181 activity has been nearly continuous since the onset of the Pu‘u ‘Ō‘ō eruption in 1983, and a
182 coincident summit eruption, characterized by a persistent plume of ash and gas and an actively
183 circulating lava lake, has been ongoing since 2008 [Orr et al., 2015].

184

185 *2.2 Piton de la Fournaise*

186 Piton de la Fournaise is a hot spot intra-plate basaltic shield volcano located on La
187 Réunion Island (Indian Ocean) and is the active surface expression of the 5000-km-long hot spot
188 chain that originated with the Deccan Trap flood basalt 65 million years ago [Duncan, 1981;
189 Morgan, 1981]. The volcano began erupting before 500 ka [Gillot and Nativel, 1989] on the
190 eastern slope of the currently inactive Piton des Neiges edifice, the base of which lies 4 km
191 below sea level on oceanic crust, and the shape of which controls the geometry of the island
192 [Lefriant et al., 2011]. Piton de la Fournaise represents less than 3% of the volume of the island
193 (which is estimated at $\sim 50,100 \text{ km}^3$) [Villeneuve et al., 2014]. The volcano is dominated by the
194 $\sim 13 \times 9 \text{ km}$ Enclos Fouqué caldera, which is approximately 4500 years old and includes a
195 terminal cone cut by two summit craters (Dolomieu and Bory; Fig. 3). The formation of the
196 Enclos Fouqué structure is controversial; four different models have been proposed: 1) polyphase
197 caldera collapse at the top of the structure accompanied by lateral eastward landsliding
198 (Bachèlery, 1981); 2) a single giant landslide (Labazuy, 1996; Oehler et al., 2004); 3) a lateral
199 eastward motion that triggered vertical collapse of the summit area (Merle and Lénat, 2003); and
200 4) downward drag related to a dense intrusive complex located 1 km depth below the eastern part
201 of the structure (Michon and Saint-Ange, 2008). Excluding subtle lineaments highlighted on
202 Digital Elevation Models [Michon and Saint-Ange, 2008] and the scars of the Osmonde paleo-
203 river (Fig. 3), no fault scarps are visible in the landscape.

204 Geochemical and geophysical data suggest the presence of several intermittently
205 connected magma reservoirs between the near surface and $\sim 11 \text{ km}$ below the summit [e.g.
206 Battaglia et al., 2005; Peltier et al., 2009; Brenguier et al., 2012; Got et al., 2013; Di Muro et al.,
207 2014]. The shallowest reservoir, from which most of the dikes feeding recent eruptions have
208 initiated, is located about 1.5–2 km depth below the summit craters [e.g. Peltier et al., 2007,
209 2008; Prôno et al., 2009].

210 Three rift zones, oriented $\text{N}10^\circ\text{--}25^\circ$ (northeast rift zone), $\text{N}160^\circ\text{--}180^\circ$ (southeast rift
211 zone), and $\text{N}120^\circ$, start from the summit and extend outside the Enclos Fouqué caldera (Fig. 3)
212 [Michon et al., 2007; Bonali et al., 2011; Saint-Ange et al., 2013]. The northeast and southeast
213 rift zones are arcuate, whereas the $\text{N}120^\circ$ rift zone is linear. The extension of the $\text{N}120^\circ$ rift zone
214 from the summit cone to the east is limited to the lower eastern slopes of the volcano, but to the
215 west it extends at least 15 km. Eruptive activity on the NW branch of the $\text{N}120^\circ$ rift zone is not

216 common, with a repeat interval of ~200 years over the last 30,000 years [e.g. Michon et al.,
217 2015]. Based on the distribution of eruptive fissures, pit craters, and cinder cones, Michon et al.
218 [2007, 2015] distinguish between upper and lower parts of the rift zones, defining “summit” and
219 “outer” segments, although the precise geometry of Piton de la Fournaise rift zones and their
220 connectivity are still debated [Michon et al., 2007; Bonali et al., 2011; Saint-Ange et al., 2013].
221 In contrast to Kīlauea, no permanent magma storage has been detected beneath or within Piton
222 de la Fournaise rift zones, which appear to only represent zones of weakness that mark preferred
223 paths for magmatic intrusions (particularly the northeast and southeast rift zones) and that bound
224 the mobile seaward eastern flank.

225 Although some phreatic and phreatomagmatic eruptions have been reported historically
226 [e.g. Peltier et al., 2012, Michon et al., 2013], eruptive activity over the past ~200 years has been
227 mostly effusive, with lava fountains and flows. Since the 18th century, 97% of all eruptions have
228 occurred within the Enclos Fouqué caldera [Villeneuve and Bachèlery, 2006], with eruptive
229 fissures opening either inside the summit Dolomieu crater (summit eruptions) or along one of the
230 rift zones (proximal and distal eruptions, the latter being located more than 5 km from the
231 summit) [Peltier et al., 2009; Roullet et al., 2012].

232 Since the Observatoire Volcanologique du Piton de la Fournaise (OVPF/IPGP) was
233 established in 1980, Piton de la Fournaise has erupted an average of 2–3 times per year, with
234 mean eruptive volumes of $8 \times 10^6 \text{ m}^3$ [e.g. Peltier et al., 2009; Roullet et al., 2012]. The magma
235 supply rate to the volcano has been estimated at 0.01–0.04 km^3/yr (Table 1) on the basis of
236 excess crustal thickness [White, 1993] and recent eruption rate [Peltier et al., 2009].

237

238 **2.3 Etna**

239 Mount Etna, the highest active volcano in Europe (3340 m above sea level as of summer
240 2007 [Bisson et al., 2016]), is a basaltic stratovolcano in eastern Sicily (Italy). The volcano is
241 located in a complex tectonic setting due to the convergence of the African and European plates
242 and also experiences flank instability [Lentini et al., 2006; Branca et al., 2011]. Etna is at the
243 front of the Apennine-Maghrebian Chain on its northern and western sides, borders the northern
244 portion of Malta Escarpment (the Mesozoic continental margin) on its eastern side, and overlies
245 clayish-sandy Pliocene-Pleistocene Catania-Gela foredeep deposits on its southern side. The
246 eastern coastline of Etna is cut by the Timpe system of normal faults, which are responsible for

247 seismicity on the lower eastern flank of the volcano (Fig 4) [Azzaro, 2004; Barreca et al., 2013;
248 Azzaro et al., 2013]. The Timpe Faults have been interpreted as the northern continuation of the
249 Malta Escarpment, which is a major lithospheric fault system separating the thick continental
250 crust of southeastern Sicily to the west from the thin oceanic crust of the Ionian Basin to the east
251 [Ben-Avraham and Grasso, 1991; Hirn et al., 1997].

252 Volcanism in the Etna region has been occurring for about 500,000 years, with scattered
253 eruptions from submarine fissures evolving to central vent activity from polygenetic centers. The
254 first transitional basaltic products clearly related to the earliest stages of the current stratovolcano
255 began erupting at about 200 ka. The present Mongibello cone, marking the summit of the
256 volcano, grew following the formation of a caldera at 15 ka. About 10 ka, the structure of the
257 volcano was radically modified by slope failures that involved a large portion of the eastern flank
258 and produced the wide depression of the Valle del Bove [Calvari et al, 2004; Branca et al.,
259 2011]. The overall volume of the Etna edifice is difficult to assess, owing to uncertain
260 knowledge of the volcano's basement; it has been estimated at 684 km³ assuming a basal plane at
261 sea level [Bisson et al., 2016]. Volcanic activity at Mt. Etna is characterized by frequent effusive
262 eruptions accompanied by persistent Strombolian activity and lava fountains with occasional
263 sub-Plinian eruptions, as indicated by both the historical and stratigraphic records [Branca and
264 Del Carlo 2004; Del Carlo et al., 2004]. Eruptions occur at or close to the summit craters
265 (summit eruptions), along flank fissures radiating from the summit sometimes to low elevations
266 (flank eruptions), and rarely from magma ascent paths that are independent of the volcano's
267 main conduit (eccentric eruptions). A higher density of eruptive fissures occur on the northeast
268 and south flanks, defining the NE and S rifts, while a wide area of eruptive vents on the west
269 flank marks the less prominent W rift. Since 1750 C.E., Etna has experienced an average of 2–3
270 flank eruptions every 25 years, but a sharp increase in this rate occurred after 1975 [Branca and
271 Del Carlo, 2004]. The past few decades have been characterized by periods of continuous
272 recharge, interrupted by lateral and summit eruptions. Harris et al. [2011, 2012] compiled and
273 calculated erupted volumes during 1980–2010 and found an average eruption rate of about 0.8
274 m³/s (0.025 km³/yr). Allard et al. [2006] estimated a similar eruption rate (0.02 km³/yr for the
275 1993–2005 period) but demonstrated from SO₂ emissions that 3-4 times more magma is
276 degassing and stored than erupted, suggesting a magma supply rate of about 0.075 km³/yr (Table
277 1). Since 2000, eruptive activity has been characterized by more frequent mild explosive activity,

278 with hundreds of episodes of lava fountaining at the summit craters, mostly from the SE crater
279 and a new vent in the vicinity [Acocella et al., 2016].

280 Geophysical data suggest that magma ascends beneath the western side of the volcano,
281 but no magma chamber has been detected [Laigle et al., 2000; Patanè et al., 2003; Bonforte et al.,
282 2008]. Seismic tomography studies have imaged a high-velocity and mainly aseismic volume
283 beneath the southeastern part of the volcano, vertically extending from sea level downwards,
284 which has been interpreted as a rigid body composed of magmatic intrusions. All pressure
285 sources modeled from ground deformation data are located along the northwestern border of this
286 body, defining an almost vertical path ranging from 9 to 2–3 km depth that projects at the surface
287 on the upper western flank of the volcano. The shallowest level of this range seems to mark the
288 level of neutral buoyancy for magma, from where intrusions can follow the main conduit of the
289 volcano towards the surface [Bonaccorso et al., 2011] or propagate as dikes away from the
290 summit, for example, as was the case in 2001 [Puglisi et al., 2008]. Magma from the central
291 conduit often intrudes radially along the two main rift zones on the upper southern and
292 northeastern flanks (Fig. 4).

293

294 **3. Characteristics of persistent flank instability at example volcanoes**

295 Despite their differing sizes, tectonic settings, eruptive styles and histories, ages, and
296 structures, Kīlauea, Piton de la Fournaise, and Etna are all affected to varying degrees by long-
297 term persistent flank instability. Structures and deposits reflect this instability in some places, but
298 the most obvious manifestation is current and ongoing surface deformation. Displacements at the
299 surface are generally accommodated by motion on subsurface fault planes or ductile transition
300 zones, but these are difficult to identify and constrain due to a lack of submarine deformation
301 data and offshore structural information. Flank instability is also modulated to some extent by
302 magmatic activity, and there is evidence for strong positive feedback between the two processes.
303 Here, we examine surface deformation, flank structure, and interaction with magmatism in an
304 effort to define the elements needed to construct a generalized conceptual framework of
305 persistent flank instability at large basaltic volcanoes.

306

307 ***3.1 Deformation***

308 At all three volcanoes, persistent ground deformation has been imaged in the form of
309 subaerial seaward surface displacements measured by the Global Navigation Satellite Systems
310 (GNSS) and Interferometric Synthetic Aperture Radar (InSAR). Motion is always on the
311 unbuttressed sides of the volcanoes in the direction perpendicular to the bounding rift zones and
312 involves motion towards the sea, but patterns of displacement vary in style between volcanoes
313 (Fig 5), which probably reflects differences in the structures that accommodate the deformation.

314 Seaward motion of Kīlauea’s south flank was first documented by broad-scale
315 trilateration surveys in the 1970s [Swanson et al., 1976], although instability was suspected from
316 structural studies and small-scale deformation measurements before that time [Moore and
317 Krivoy, 1964]. The use of GNSS considerably elucidated understanding of flank displacements,
318 providing a comprehensive four-dimensional perspective of surface motion [Owen et al., 1995,
319 2000a; Brooks et al., 2006]. The unstable flank is bounded to the north by Kīlauea’s rift zones,
320 the north sides of which are apparently stable (Fig. 5a) [Owen et al., 1995]. Seaward horizontal
321 displacements south of the rift zones range from a few cm/yr on the south margins of the summit
322 caldera and rift zones to ~8 cm/yr at the south coast [Owen et al., 2000a]. Vertical deformation at
323 the summit and along the rift zones varies over time according to magmatic activity, but uplift
324 characterizes the south coast (Fig. 5a, 6) [Owen et al., 2000a; Peltier et al., 2015a]. Although the
325 south flank of the volcano is cut by the Hilina and Koa‘e fault systems (Fig. 2), there is little
326 evidence to suggest that these faults divide the flank into blocks that move independently
327 between major earthquakes (modeling of InSAR data by Shirzaei et al. [2013] that argues such
328 has yet to be confirmed by additional observations). Seaward flank motion is remarkably steady
329 in time, at least since 1995, when continuous GNSS monitoring was initiated [Miklius et al.,
330 2005]. The steady motion is interrupted by two processes (Fig. 6): 1) rift zone intrusions [e.g.,
331 Lundgren et al., 2013], which cause compression on the flank that may lead to strong
332 earthquakes [Swanson et al., 1976; Poland et al., 2008], and 2) slow slip events (SSEs), which
333 occur quasi-periodically and involve moment release equivalent to a ~M5–6 earthquake but
334 spread over 24–48 hours, with minor accompanying seismicity [Cervelli et al., 2002a; Brooks et
335 al., 2006; Segall et al., 2006; Wolfe et al., 2007; Montgomery-Brown et al., 2009, 2015].

336 At Piton de la Fournaise, even though eastward lateral spreading had long been suspected
337 (based on the asymmetrical pattern of summit and near-summit deformation [e.g. Peltier et al.,
338 2007, 2008; Derrien et al., 2015]), it was only confirmed in the mid-2000s, when up to 1.4 m of

339 seaward motion was measured by InSAR on the volcano's east flank during the April 2007 distal
340 eruption [e.g. Tinard, 2007; Clarke et al., 2013; Froger et al., 2015]. Unfortunately there were no
341 permanent GNSS stations on the flank at the time of that eruption, so it is not possible to
342 discriminate between cause and the consequence—in other words, are distal eruptions a
343 consequence of seaward slip (Got et al., 2003), or is seaward slip a consequence of the distal
344 eruption (e.g. Chaput et al., 2014; Froger et al., 2015)? Subsequent flank deformation, including
345 during inter-eruptive periods, has been measured by systematic InSAR acquisitions (national
346 monitoring system OI2, <http://www.opgc.univ-bpclermont.fr/SO/televolc/volinsar/indexEN.php>,
347 Clermont Ferrand University; CASOAR database) and the installation of six permanent GNSS
348 stations on the eastern flank of the volcano in 2009–2010 (via the ANR-08-RISK-011
349 UnderVolc project) (Fig. 5b) [Brenguier et al., 2012; Got et al., 2013; Peltier et al., 2015b]. Since
350 they were established, four of the six permanent GNSS stations (located in the middle and
351 southern part of the eastern flank) recorded continuous eastward motion (of about 1.4 cm/yr) and
352 subsidence (up to ~2.5 cm/yr) [Brenguier et al., 2012; Peltier et al., 2015b; Staudacher and
353 Peltier, 2016]. Much of the subsidence is due to contraction of recent lava flows on which the
354 stations are installed; the stations on the youngest lava flows have the greatest subsidence rates
355 [Peltier et al., 2015b]. During the 2010–2014 inter-eruptive period, eastward velocities recorded
356 on these four stations were quite similar (Fig. 5b). The two remaining GNSS stations, located in
357 the northern part of the east flank, are decoupled from the others by paleostructures delimiting
358 the Plaine des Osmondes collapse and Osmondes paleoriver (Fig. 3) [e.g. Courteaud, 1996;
359 Michon and Saint-Ange, 2008] and did not record clear eastward motion, especially during inter-
360 eruptive periods (< 3 mm/yr; Fig. 5b). Among these two stations, only the closest to the terminal
361 cone recorded significant deformation during magmatic unrest in 2015. Seismicity on the eastern
362 flank is sparse, with only a few low-magnitude events detected at about 2 km below sea level
363 beneath the Grandes Pentes area (Fig. 3).

364 Like Piton de la Fournaise, Etna is characterized by eastward motion of its east flank
365 (Fig. 5c). Starting in the 1990s, structural, geodetic and seismotectonic investigations suggested
366 that a large portion of the eastern flank of Etna was sliding towards the sea [Borgia et al. 1992;
367 Patanè et al. 1994; McGuire et al. 1996; Rust and Neri 1996; Houliè et al., 2006]. During the
368 2000s, deformation measurements quantified the flank motion to have a mean rate of about 2–3
369 cm/yr, but with a maximum of about 3–5 cm/yr along the coast and northeast flank, variable in

370 space and time [Solaro et al., 2010; Bonforte et al., 2011]. Seismic and geodetic data indicate
371 that the unstable flank is composed of several blocks with faults and fractures along their borders
372 and that are characterized by distinct earthquake and displacement patterns [Bonforte and
373 Puglisi, 2006; Solaro et al., 2010; Bonforte et al., 2011]. The northern boundary of the unstable
374 sector is the Pernicana fault, which cuts the entire NE flank of the volcano from the NE rift zone
375 to the sea (Fig. 4). The fault shows a mostly left-lateral mean slip rate of about 2.5–3 cm/yr, but
376 that rate can increase suddenly during magmatic events, when tens-of-cm-scale displacements
377 and seismic swarms occur over the course of a few days [Bonforte et al., 2007a; Guglielmino et
378 al., 2011; Ruch et al., 2013]. The rate of seaward flank motion decreases to the south across a
379 number of faults with NNW-SSE and WNW-ESE trends [Azzaro et al., 2013; Barreca et al.,
380 2013]. All faults on the southern slope of the volcano start from the south rift and continue to the
381 sea, curving from a NNW-SSE azimuth with mostly normal motion on the upper slopes to an
382 almost E-W orientation with mainly transcurrent kinematics at the coast [Bonforte et al., 2011].
383 The Trecastagni fault (Fig. 4) represents the main southern boundary of the sliding eastern sector
384 [Gambino et al., 2011; Bonforte et al., 2011, 2013a], with reduced displacements across the
385 southern slope of the volcano and accommodated by other less evident structures [Barreca et al.,
386 2013; Bonforte et al., 2013b]. The entire southern sector of the volcano shows minor spreading
387 motion, and the Ragalna fault (Fig. 4) represents the boundary of this sector on the southwest
388 side of the volcano [Bonforte et al., 2011; Neri et al., 2007].

389

390 **3.2 Flank structure**

391 The structures of the mobile flanks on Kīlauea, Piton de la Fournaise, and Etna span the
392 entire range of potential complexity, from a lack of exposed faults at the surface of Piton de la
393 Fournaise, to the fault-bounded blocks of Etna. Unfortunately, the sliding surfaces that
394 accommodate flank motion are poorly known in the cases of Etna and Piton de la Fournaise
395 owing to a paucity of seismicity and a lack of deformation and structural data from the
396 submarine flanks of the volcanoes.

397 At Kīlauea, the Koa‘e and the Hilina fault systems dominate the volcano’s subaerial
398 south flank. The depth of faulting in the Koa‘e is ambiguous, with evidence suggesting both
399 shallow (upper several hundred meters) and deep (~10 km) extents [Duffield, 1975]. Initially, the
400 depth of the Hilina faults was debated, with some workers speculating that the faults were the

401 headwall of a large landslide [e.g., Moergan et al., 2000], while others argued that the faults cut
402 the entire volcanic pile to its base, ~8 km below sea level [e.g., Lipman et al., 1985]. Ground
403 deformation and fault displacements associated with the 1975 Kalapana earthquake, however,
404 seem to favor the shallow model for the fault system [e.g., Cannon and Bürgmann, 2001].
405 Overall displacement of Kīlauea’s south flank occurs due to motion on a basal décollement that
406 lies at the boundary between the volcanic pile and preexisting oceanic crust, coupled with
407 opening of Kīlauea’s rift zones [Delaney et al., 1990]. The subhorizontal detachment fault is
408 defined by seismicity [e.g., Got and Okubo, 2003; Matoza et al., 2013] and suggested by
409 compressional structures in the submarine portion of the flank [Morgan et al., 2000]. The
410 detachment appears to be actively creeping adjacent to the rift zones and locked offshore
411 [Montgomery-Brown et al., 2015]. Such a kinematic model explains secular flank motion (due to
412 the creeping section), strong earthquakes (due to the locked section), and aseismic slip events
413 (which occur along the transition between the locked and creeping sections). The depth of the
414 décollement has been a source of some debate, since geodetic models are poorly constrained due
415 to the scarcity of offshore deformation data. Joint consideration of seismic and geodetic data,
416 however, favor a depth of ~8 km [Segall et al., 2006] (although the seismic data permit shallower
417 depths as well [Wolfe et al., 2007]), which is also supported by limited submarine vertical
418 displacement data [Phillips et al., 2008]. The position of the fault at the interface between the
419 volcano and ocean crust is consistent with the presence of weak marine sediments at this
420 boundary [Nakamura, 1980; Dieterich, 1988] due to the advanced age of the plate (~95 million
421 years) [Van Ark and Lin, 2004]. Thus, Kīlauea’s unstable flank appears to be underlain by a
422 décollement fault at the base of the volcanic pile that transitions from onshore slipping to
423 offshore locked, while at shallower depths the flank hosts normal faults that respond to sudden
424 flank movements.

425 In contrast to Kīlauea, there is no clear evidence of a décollement plane below the
426 unstable flank of Piton de la Fournaise, although structural discontinuities are suggested by
427 geological and geophysical data. A geological boundary, indicated by a low-seismicity zone and
428 the depth of the upper magma reservoir [e.g. Peltier et al., 2008, 2009; Prôno et al., 2009],
429 appears to be present at sea level [Battaglia et al., 2005], suggesting a neutral buoyancy surface.
430 A few earthquakes have been recorded in the Grandes Pentes area of the east flank, about 2 km
431 below sea level (in 2016, ~10 $M < 2$ events were relocated in this region, although the rest of the

432 volcano's east flank is mostly aseismic), which may be the continuation of a structure marked
433 by a low-seismicity zone beneath the summit observed during migration of earthquakes prior to
434 the 1998 eruption [Battaglia et al., 2005]. According to Gailler et al. [2009], the top of the
435 intrusive layered complex, encountered by a drill hole in the Grand Brûlé area of the lower
436 eastern flank (from about 830 m bsl to 2830 m bsl), could be a glide plane overlain by landslide
437 products, as suggested by Courteaud [1996]. Geologic evidence from Piton des Neiges and
438 modeling of geodetic data at Piton de la Fournaise guided by those constraints argue that
439 shearing of a magmatic sill that was intruded along a detachment fault could explain the large
440 flank displacements associated with the 2007 distal eruption at the volcano [Chaput et al., 2014],
441 with continued seaward displacements as the co-eruptive motion decays slowly over time. The
442 modeled size of such a sill, however, is not realistic, suggesting that a fault plane is a more viable
443 source of east flank motion [Tridon et al., 2016]. The speculated detachment surface, regardless
444 of its form, is probably not at the interface of the volcanic pile and sea floor, which is 7–8 km
445 beneath the volcano's summit, but might be at the interface between Piton de la Fournaise and
446 the underlying Piton des Neiges, although there are no compressional structures analogous to
447 those on Kīlauea's submarine flank suggesting such a fault plane [Le Friant et al., 2011]. The
448 possibility of a detachment plane beneath the east flank of Piton de la Fournaise therefore
449 remains ambiguous. Another major difference between Piton de la Fournaise and Kīlauea is the
450 lack of surface faulting and relatively simple flank structure on the former.

451 If Piton de la Fournaise represents the simple end member of flank structure, Etna trends
452 towards the more complex end of the spectrum. Etna's mobile sector is heavily faulted due to the
453 numerous blocks that make up the flank. The most significant flank faults are the NNW-SSE-
454 striking Timpe faults, which usually show normal motion but are also occasionally characterized
455 by reverse displacements [Puglisi et al., 2008]. The latter behavior is usually associated with an
456 "active pushing" of the mobile flank by dike intrusions [Puglisi et al., 2008] as suggested by 2D
457 analogue experiments [Le Corvec et al., 2014], but has also been observed on the Pernicana
458 fault, which defines the northern boundary of the unstable flank, in association with strong
459 summit inflation [Puglisi et al., 2001; Bonforte et al., 2007a]. Off-shore investigations [Chiocci
460 et al., 2011; Gross et al., 2015] indicate that the continental margin is affected by a wide
461 semicircular fault system that can be interpreted as the expression of a large-scale retrogressive
462 instability extending to a depth of more than 2000 m. Based on these data, we suggest that the

463 on- and off-shore portions of the Timpe fault system are part of the flank instability affecting the
464 continental margin, rather than the northernmost extension of the Malta Escarpment. This
465 interpretation is consistent with GNSS surveys that demonstrate the involvement of the Timpe
466 faults in the eastward motion of the flank [Bonforte and Puglisi, 2006].

467 The thickness of the sliding pile on Etna's east flank is not clear. It surely involves the
468 upper part of the sedimentary basement, which outcrops on the mobile part of the northeastern
469 flank up to an altitude of 800 m a.s.l. Conceptual models of the flank suggest a U-shaped sliding
470 sector with a base that may lie between sea level and several kilometers below sea level [Froger
471 et al., 2001; Azzaro et al., 2013, and references therein]. Geophysical data (seismicity,
472 tomography, and resistivity) have not identified a zone of weakness beneath the flank [De Gori et
473 al., 2005; Siniscalchi et al., 2012] but do suggest a change in the pattern of the stress field at ~2-3
474 km b.s.l. [Alparone et al., 2011]. The depth of a hypothetical detachment level has been inferred
475 only from geological evidence and inversion of ground deformation measured by GNSS. On the
476 middle of the northeastern flank, both geology and geodesy indicate compressional features
477 along the lower half of the Pernicana fault system that may be related to a shallow décollement
478 and/or to rotation of the fault with respect to the motion of the flank [Tibaldi and Groppelli,
479 2002; Bonforte et al., 2007a]. A deeper sliding plane—at sea level or below—must also exist,
480 given ground deformation measured along the coastline. The depth of such a plane is not easy to
481 model, owing to a lack of seismicity and offshore geodetic data. Two depths have been
482 suggested from inversion of ground deformation data: 1) a deep detachment at 2–3 km b.s.l. that
483 involves a thick portion of the sedimentary basement, suggested also by deformation associated
484 with the 2001 flank eruption [Bonforte and Puglisi, 2006; Bonforte et al., 2009; Ruch et al.,
485 2010; Le Corvec et al., 2014], and 2) a shallower detachment at 0–2 km b.s.l, based on post-
486 eruptive deformation following activity in 2001 and in 2002, when flank motion at sea level
487 accelerated dramatically, models of which require the involvement of the volcanic pile and the
488 uppermost levels of the sedimentary basement [Bonaccorso et al., 2006; Bonforte et al., 2008].

489

490 ***3.3 Interaction with magmatic activity***

491 On all the three volcanoes, seaward motion of the unstable flanks is modulated by
492 magmatic activity. The degree to which magmatic process influence flank instability, however,

493 varies in intensity from being a secondary trigger of ongoing flank motion (at Kīlauea) to being a
494 primary control on the rate of flank slip (at Piton de la Fournaise).

495

496 3.3.1 Quiescent periods

497 “Quiescence” has been largely unknown at Kīlauea since an 18-year period of no
498 eruptions came to an end in 1952. Especially starting with the advent of flank deformation
499 measurements in the 1960s, the volcano has been in a state of constant magmatic activity—if it
500 was not erupting, magma was accumulating beneath the summit [Wright and Klein, 2014]. The
501 closest thing to quiescence might be relatively steady periods of the 1983–present Pu‘u ‘Ō‘ō
502 eruption, when the eruption rate was comparatively constant for months to years at a time and
503 summit deformation was deflationary, indicating that most magma entering the volcano was
504 being transported to the eruption site [Kauahikaua and Miklius, 2003]. During such periods,
505 flank motion was mostly steady, ~8 cm/yr along the coast [Owen et al., 2000a], except during
506 SSEs. Presumably occurring on the décollement at the transition between the creeping and
507 locked portions of the fault, SSEs manifest a periodicity and can be separated into different
508 spatial families [Brooks et al., 2006; Montgomery-Brown et al., 2015]. Since 2003, the events
509 have been larger in magnitude and more periodic in occurrence (2.44 ± 0.15 years)
510 [Montgomery-Brown et al., 2015]. The often steady motion of the flank and regular occurrence
511 of SSEs, regardless of the magmatic state of the volcano, imply that gravitational spreading is a
512 major driving force of flank deformation. Swanson et al. [1976] speculated that flank motion
513 could be driven by dike intrusion in the shallow rift zone, and such activity undoubtedly does
514 have an impact on short (months to years) timescales, but an alternative mechanism is the flow
515 of dense olivine cumulates beneath the summit and within the deep rift zones [Clague and
516 Denlinger, 1994]. In fact, numerical modeling indicates that gravitational spreading due to flow
517 of dense cumulates can explain long-term secular deformation of Kilauea’s south flank [Plattner
518 et al., 2013]. Overprinted on this long-term gravitational spreading are transient magmatic events
519 that were encouraged by persistent flank motion. Dike intrusions in 1997 [Owen et al., 2000b]
520 and 1999 [Cervelli et al., 2002b] were ascribed to a decrease in the least compressive stress
521 across the East Rift Zone owing to seaward flank motion, and SSEs are associated with, and
522 might have triggered, some anomalous magmatic activity [Montgomery-Brown et al., 2015].

523 Quiescence is more common at Piton de la Fournaise and Etna, where it is manifested as
524 a lack of eruptive activity and summit deflation that can persist for months to years. During the
525 2010–2014 non-eruptive period at Piton de la Fournaise, seaward motion was relatively steady
526 (Fig. 6), although the behavior of the flank during previous quiescent times is not known owing
527 to a lack of deformation data in this sector before 2010. Summit deflation and seaward-directed
528 flank motion generates extension within the upper part of the eastern flank [Peltier et al., 2015b].
529 The situation is much the same at Etna (and Kīlauea), where the east flank moves toward the sea
530 along the coast even when the volcano is not erupting or inflating. Summit deflation combined
531 with flank spreading seems to produce a relaxation of the mobile flank, prompting motion along
532 local faults and causing extension along the NE rift [Bonforte et al., 2008].

533

534 3.3.2 Periods of magmatic unrest

535 At Kīlauea, magmatic activity does not appear to affect the steady long-term seaward
536 motion that has characterized the volcano’s southern flank since the start of continuous geodetic
537 observations in the 1990s. For example, during a surge in magma supply in 2003–2007, when the
538 amount of magma entering the volcano from the mantle more than doubled and inflation was
539 detected at the summit and along the rift zones, there was no significant change in flank
540 displacement rates [Poland et al., 2012, 2014; Anderson and Poland, 2016]. Similarly, no change
541 in the long-term displacement rate of coastal GPS stations was observed following other dike
542 emplacement events in the rift zones, like that of 2011 (Fig. 6). Magmatic activity has, however,
543 been observed to trigger short-term transient flank motion in two ways. First, intrusion into, and
544 spreading of, the rift zones, if occurring at a faster rate than flank spreading, causes compression
545 of the flank. Swanson et al. [1976] recognized this condition from deformation data in the 1970s
546 and speculated that an earthquake might result. It is also relatively common for M~5 events to
547 occur on the décollement beneath the flank in the days to weeks after rift zone intrusions and
548 dike-fed fissure eruptions, again likely due to flank compression [e.g., Poland et al., 2008].
549 Second, SSEs have been associated with magmatism. The best example is the Father’s Day
550 intrusion and eruption of June 2007, when a dike intruded the volcano’s East Rift Zone at about
551 the same time that an SSE was expected (based on the occurrence of SSEs in 2003 and 2005).
552 Dike growth, which was initially caused by magma overpressure at the summit, appeared to be
553 waning after ~6 hours of activity when an SSE began, perhaps encouraged by the opening of the

554 initial dike as suggested by stress modeling [Brooks et al., 2008; Montgomery-Brown et al.,
555 2010]. Flank slip facilitated further rift zone opening and the reinvigoration of the intrusion,
556 resulting in the emplacement of a second, larger dike that ultimately reached the surface [Brooks
557 et al., 2008; Poland et al., 2008; Montgomery-Brown et al., 2010, 2015]. This reinvigoration was
558 a consequence of a decrease in the least compressive stress across the rift zone caused by the
559 SSE as opposed to magma overpressure. Magmatic activity has also been associated with the
560 occurrence of SSEs in 2005 and 2012; thus, it appears that SSEs and Kīlauea’s magmatic system
561 have the potential to influence one another, but only if either or both of those systems are already
562 close to failure [Montgomery-Brown et al., 2015]. Large flank slip events also have an obvious
563 impact on eruptive and intrusive activity at Kīlauea, as demonstrated by the 1975 earthquake,
564 which created a situation favoring intrusion over eruption for months to years after the
565 earthquake [Dzursin et al., 1980]. Previous episodes of flank slip were associated with similar
566 major changes in eruptive and intrusive behavior [Denlinger and Morgan, 2014].

567 In stark contrast, flank motion at both Piton de la Fournaise and Etna responds to changes
568 in magmatic activity—specifically, seaward flank motion accelerates during periods of inflation
569 and eruption [e.g., Bonforte et al., 2008; Bonaccorso et al., 2011; Peltier et al., 2015b; Chen et
570 al., in revision]. For example, at Piton de la Fournaise, steady seaward motion accelerated in
571 2015 across the entire east flank simultaneous with a deep seismic swarm (7 to 1.5 km bsl) 31
572 days prior to the May 17 eruption, and higher flank motion rates persisted until the onset of the
573 August 24 eruption [Peltier et al., 2016]. Dike emplacement at Piton de la Fournaise is often
574 characterized by an asymmetrical pattern, with seaward motion of the eastern flank and almost
575 no motion of the western flank. This condition has resulted in net displacements of 9.2 ± 2.5 m
576 of displacement to the east and 1.3 ± 2.5 m to the west during 1950–2015 [Derrien et al., 2015].
577 Distal eruptions are associated with especially significant flank motion, exemplified by the 1.4 m
578 of seaward displacement observed during April 2007 [Froger et al., 2015]. Got et al. [2013]
579 showed that such large plastic motion relaxed the horizontal elastic stress accumulated during the
580 periods between distal eruptions and facilitated lateral transport of magma to eruption sites far
581 from the summit. This strain weakening of the edifice may occur along a plane at depth that
582 favors sill formation, as proposed by Chaput et al. [2014], although Tridon et al. [2016] favor a
583 detachment surface.

584 At Etna, spreading of the volcano is also clearly enhanced by summit inflation, which
585 promotes accelerated eastward motion of the eastern flank. The inflation is sometimes strong
586 enough to cause the mobile flank to overthrust the stable portion of the volcano, as indicated by
587 the reverse motion of some flank faults [Puglisi et al., 2001; Le Corvec et al., 2014]. This is part
588 of a feedback process [Acocella et al., 2003; Bonaccorso et al., 2011; Alparone et al., 2013],
589 much like that observed in 2007 at Kīlauea, where seaward flank motion encourages magma
590 ascent, and also as has been proposed at Piton de la Fournaise to explain distal eruptions [Got et
591 al., 2013]. The feedback can be strong enough that some lateral eruptions are considered to be
592 favored or triggered by the flank motion, with stored magma erupting from extensional fractures
593 caused by stretching induced by the spreading [Bonaccorso et al., 2006]. Forceful dike intrusion
594 can also provide a “push” to the flank. In the long-term, both “active” (i.e., triggered by magma
595 overpressure) and “passive” (i.e., triggered by rift opening) processes have been observed as part
596 of a continuous feedback between flank motion and magma dynamics [Alparone et al., 2013;
597 Acocella et al., 2016]. Lateral and eccentric dike intrusions strongly modify the local stress
598 pattern at Etna and, consequently, modulate spreading of the mobile sector of the volcano. In
599 2001, for example, the intrusion of an eccentric dike on the upper south flank of the volcano was
600 part of a positive feedback with instability of the eastern flank [Billi et al., 2003; Bonforte et al.,
601 2009]. Deformation data indicate that a flank fault that slipped in one direction during the
602 intrusion reversed its direction of slip during the subsequent eruption, and after a few weeks an
603 increase in lower flank seismicity and seaward motion occurred [Puglisi et al., 2008]. In contrast
604 to 2001, the 2002 intrusion on the NE rift was at least partially promoted by flank motion that
605 caused extension across the rift, especially its upper part, as indicated by deformation and gravity
606 data [Bonforte et al., 2007b; Ruch et al., 2012]. The reaction of the mobile flank to the 2002
607 intrusion included large and immediate displacements along the Pernicana fault [Bonforte et al.,
608 2007a; Alparone et al., 2013] and, after a few days, also of other faults that dissect the sliding
609 flank [Acocella et al., 2003]. The intrusion of the dike that fed the 2008-09 eruption was partially
610 controlled by flank dynamics [Bonforte et al., 2013c], while, in turn, a very shallow dike
611 intrusion in 2014 seems to have come close to triggering a slope failure on the upper part of
612 Valle del Bove [Bonforte and Guglielmino, 2015].

613

614 **4. Conceptual framework for persistent flank instability**

615 The above review of flank characteristics at Kīlauea, Piton de la Fournaise and Etna
616 highlights the strong relation that exists between the factors controlling long-term persistent
617 flank instability (gravitational and magmatic forces, as well as structural setting) and its
618 expression at surface. These three volcanoes define a broad spectrum in terms of these factors
619 (Table 1), and this range is responsible for the observed differences in the manifestations of
620 ongoing flank deformation.

621

622 *4.1 The spectrum of persistent, long-term instability*

623 Even though the overall deformation style on the three volcanoes we reviewed is
624 similar—persistent seaward displacement of the unbuttressed flank in the direction perpendicular
625 to the bounding rift zones—the characteristics of the deformation are quite different. Flank
626 faulting varies widely, with Etna displaying independently moving blocks, Kīlauea with fault
627 systems that respond to large earthquakes but possibly not to steady creep, and no visible major
628 faulting on the mobile flank of Piton de la Fournaise. The displacement rates vary as well, being
629 much higher at Kīlauea, which has the highest magma supply and is the largest edifice of the
630 three (Fig. 6, Table 1). The surfaces that accommodate the motion may also be very different. At
631 Kīlauea, flank slip occurs along the boundary between the preexisting ocean floor and the
632 volcanic pile, lubricated by the presence of weak oceanic sediments. The sliding surfaces at Piton
633 de la Fournaise and Etna are much less well known owing to a lack of geophysical evidence that
634 strongly delineates the presence of a plane of weakness. Flank slip at Piton de la Fournaise could
635 occur on either a sheared sill, as seen on Piton des Neiges [Famin and Michon, 2010; Chaput et
636 al., 2014], or a detachment fault [Cayol et al., 2014; Tridon et al., 2016], perhaps along a
637 geological boundary of some sort [Got et al., 2013]. Slip of Etna’s flank may also be
638 accommodated along a fault at unknown depth and involves some portion of the volcano’s
639 sedimentary basement. While the depths vary significantly (8–10 km beneath the surface at
640 Kīlauea to possibly less than a few km at Piton de la Fournaise and Etna), in all three cases the
641 slip plane is probably associated with a weak boundary layer, be it sediment, a sill, or some other
642 geological discontinuity. Weak sedimentary layers or geological boundaries have long been
643 highlighted as necessary factors in accommodating volcanic spreading [e.g., Borgia et al.,
644 1992, 2000], and appear critical for supporting long-term persistent instability at large basaltic
645 edifices.

646 The varying role of magma pressure versus gravitational spreading in flank processes
647 appears to correlate with the size of the volcano. Kīlauea experiences steady flank motion that
648 can be explained as primarily due to gravitational spreading [Clague and Denlinger, 1994;
649 Plattner et al., 2013], perhaps because the volcano is the largest of the three we examined (Table
650 1) and has a dense core. Magmatic activity is a secondary factor that influences flank processes
651 only when the décollement is already close to failure (e.g., when an SSE is about to occur
652 anyway [Montgomery-Brown et al., 2015]) or if flank is temporarily put into a state of
653 compression [Swanson et al., 1976]. Similarly, flank slip impacts the magmatic system when
654 magma is already primed for eruption or intrusion, as with the buildup of rift zone extension
655 prior to the 1997 and 1999 dike intrusions [Owen et al., 2000b; Cervelli et al., 2002b], or during
656 the 2007 intrusion-SSE-intrusion sequence [Montgomery-Brown et al., 2010, 2015]. Flank
657 instability at both Piton de la Fournaise and Etna, in contrast, is characterized by a much stronger
658 response to changing magmatic conditions, with episodes of flank motion being triggered by,
659 and further triggering, eruptive and intrusive activity. At all three volcanoes, rift zones play an
660 important role by defining the boundary of the unstable flank, with little motion on the “stable”
661 side. Rift zone development is strongly tied to instability [e.g., Walter et al., 2005], given the
662 strong positive feedback between rift opening and flank displacements [e.g., Poland, 2014a], due
663 to the buildup of steep, unstable slopes, especially in triple-armed rifts [Carracedo, 1999], or
664 from volcanic spreading as a factor in rift zone formation [Münn et al., 2006].

665 Although catastrophic collapse is widespread among large volcanic edifices, persistent,
666 long-term instability has been identified on only a few volcanoes worldwide. In addition to
667 Kīlauea, Piton de la Fournaise, and Etna, Mauna Loa has a steadily moving flank. The rate of
668 motion (a few cm/yr) is intermediate between Kīlauea and Etna but is occurring on the flank that
669 abuts Kīlauea [Miklius et al., 1995]—a testament to the size of Mauna Loa and the gravitational
670 force driving the instability (apparently, even buttressed flanks can creep given enough force,
671 although Kīlauea is growing on the flank of Mauna Loa, and its volume is a small fraction of
672 Mauna Loa’s [Lipman and Calvert, 2013]). Flank creep of a few mm/yr has also been
673 documented using a large InSAR dataset at Cumbre Vieja volcano, La Palma, Canary Islands,
674 where the deformation may be due to sliding along buried sediments or debris avalanche deposits
675 [González et al., 2010]. Structural studies have suggested flank creep at other volcanoes as well,
676 like Mt. Cameroon, west Africa [Mathieu et al., 2011], although no geodetic results have

677 confirmed this possibility (it may be that such deformation is below detection thresholds, except,
678 perhaps, when the volcano enters a period of magmatic unrest). Flank creep was suspected at
679 Fogo, Cape Verde Islands, on the basis of structural studies of the 1951 and 1995 eruptions [Day
680 et al., 1999], but there was no evidence from geodetic studies of the 1995 [Amelung and Day,
681 2002] or 2014–2015 [González et al., 2015] eruptions to corroborate this hypothesis. Fogo,
682 however, is characterized by a collapse scar on its east flank—indeed, many ocean island
683 volcanoes without persistent motion show evidence of catastrophic collapse, like Tristan da
684 Cunha and El Hierro [Holcomb and Searle, 1991]. The Sciara del Fuoco scar on the northwest
685 flank of Stromboli volcano is a result of a huge sector collapse [Tibaldi, 2001], and there is
686 downslope motion of that flank that is modulated by eruptive activity [Di Traglia et al., 2014],
687 but the motion appears to be related to the stability of lava flows on this steep slope [Bonaccorso
688 et al., 2009; Bonforte et al. 2016]. Past collapses on these volcanoes may have been associated
689 with persistent flank motion prior to failure, although this remains speculative without
690 supporting models or observations. At all volcanoes where persistent flank motion has been
691 documented or hypothesized, the moving flank is along the coast (even at non-ocean-island
692 volcanoes, like Etna) and largely unbuttressed by significant topography. While such a condition
693 may not be sufficient to cause persistent flank motion, it may be necessary to sustain long-term
694 instability [e.g., Froger et al., 2001; Norini and Acocella, 2011].

695

696 ***4.2 Factors controlling persistent flank instability***

697 From our comparative analysis, the occurrence of long-term continuous flank instability
698 at large basaltic volcanoes seems to require at least two conditions: (1) the presence of a weak,
699 subhorizontal layer within the subsurface upon which sliding can occur, and (2) gravitational
700 spreading and/or magmatic force to cause internal edifice strain weakening and motion along the
701 weak layer (such force may be counteracted by the buttressing presence of an adjacent volcano
702 or other topography, explaining why persistent instability has thus far only been observed in
703 island and coastal environments). This conclusion is not new. Many other authors have
704 recognized the combination of gravitational/magmatic loading and weak basement on volcanic
705 spreading [e.g., van Wyk de Vries and Borgia, 1996; Borgia et al., 2000]. The combination of
706 these factors, however, must be relatively rare when it comes to large basaltic edifices, given the
707 global paucity of persistent flank instability on such volcanoes. It may therefore be helpful to

708 define a framework for long-term flank instability of large basaltic volcanoes based on these
709 factors as a means of understanding why a particular volcano may or may not be characterized
710 by persistent flank motion.

711 Subhorizontal planes of weakness can have numerous forms, and their presence seems to
712 depend largely upon the setting in which a volcano grows. Sediment on old oceanic plates
713 provides a lubricating layer upon which sliding could occur, as is the case in Hawai‘i, where the
714 Pacific Plate is about 95 million years old. Although Piton de la Fournaise is also located on an
715 old oceanic plate (~66 million years old), it is growing on the flank of the preexisting Piton des
716 Neiges volcano. The interface between the two edifices provides a boundary layer upon which
717 flank sliding may occur in this case, although it is also possible that a sill intrusion or layered
718 intrusive complex is the weak layer. Unlike the other two volcanoes, Etna lies at a convergent
719 margin, where sedimentary basement rocks are a likely source of weakness beneath the sliding
720 east flank. Volcanoes that do not have thick weak layers beneath them seem to be less prone to
721 long-term persistent flank instability (although not necessarily less prone to catastrophic
722 collapse). For instance, the volcanoes of the western Galápagos have grown simultaneously upon
723 ~10-million-year-old ocean floor with little sedimentary cover, so there is no obvious weak layer
724 beneath any of the volcanoes (in addition, the volcanoes buttress one another, except on the
725 western sides of the western-most volcanoes) [Nakamura, 1980; Chadwick and Dieterich, 1995;
726 Poland, 2014a]. In this light, the lack of creep on volcanic flanks in the Galápagos is not
727 surprising.

728 When a weak layer is present, the force needed to drive persistent flank instability can be
729 provided by gravitational spreading and/or magmatism. To be dominated by gravitational
730 spreading requires that a volcano be massive, which in turn implies a very high rate of magma
731 supply to the edifice and/or a slow rate of plate motion (which governs the amount of time that a
732 volcano is connected to its magma source in the case of hotpot volcanoes). Hawai‘i is the only
733 case of the three studied here where, thanks to the great rate of melt production, volcanoes can
734 grow in size to tens of thousands of km³ despite the relatively fast motion of the Pacific Plate
735 (Table 1), which limits vigorous volcanism at a given volcano to few hundred thousand years
736 [Lipman and Calvert, 2013; Clague and Sherrod, 2014]. The importance of melt production is
737 evident in comparing Kīlauea and Piton de la Fournaise—Kīlauea is an order of magnitude larger
738 in volume, owing to its higher magma supply rate, yet Piton de la Fournaise is longer lived, since

739 it sits on a much more slowly moving plate (Table 1) [Peltier et al., 2015a]. The rapid flank
740 motion at Kīlauea may therefore be a natural consequence of, and provide a balance for, the high
741 and continuous magma supply to the volcano, which constructs a massive edifice. At smaller
742 volcanoes, like Etna and Piton de la Fournaise, magmatic forces play a larger role in the
743 occurrence of long-term flank instability, as demonstrated by the correlation between changes in
744 flank motion rate and intrusive/eruptive activity. In fact, flank instability at Piton de la Fournaise
745 and Etna may be a geologically recent phenomenon. The contemporary magma supply to both
746 volcanoes is an order of magnitude higher than their overall growth rates (edifice volume divided
747 by volcano age; Table 1), so current high rates of magma supply to both volcanoes (relative to
748 their overall growth rates) might drive current flank motion. Regardless, a common factor among
749 all three volcanoes is high, and quasi-continuous, magma supply, which therefore seems a strong
750 factor in developing and sustaining long-term persistent instability.

751 An examination of the relationships between maximum flank displacement rate, edifice
752 size, and magma supply supports the inference that volcanoes with high rates of magma supply
753 are most prone to develop persistent flank instability, with edifice size also playing a role
754 (especially in the case of gravitational spreading versus magma-driven flank motion; Fig. 7).
755 Cumbre Vieja does manifest flank instability despite its low magma supply rate (probably
756 similar to that of nearby El Hierro—about $0.002 \text{ km}^3/\text{yr}$ [González et al., 2013]—based on
757 comparable recent eruptive history) and has a volume of several thousand km^3 [Schmincke,
758 1982], and the flank may be underlain by debris avalanche or sedimentary deposits [González et
759 al., 2010]. The lack of magmatic activity coincident with the observed flank deformation
760 suggests that a weak layer plus the volcano's size may be sufficient to drive a small amount of
761 persistent flank motion (volcanoes with similar sizes and magma supply rates, like El Hierro and
762 Fogo, have experienced catastrophic collapses, possibly removing flanks that were subject to
763 persistent motion). Conversely, some Galápagos volcanoes have comparatively high rates of
764 magma supply but no persistent flank motion, emphasizing the importance of a weak substrate
765 for sustaining instability.

766

767 ***4.3 Long-term persistent flank instability: a conceptual framework***

768 Given the relationships between magma supply, edifice size, and volcanic basement, a
769 useful framework for understanding long-term persistent flank instability may be the interplay

770 between the structural setting of a volcano, which governs the presence and thickness of any
771 underlying weak layer, and the magmatic activity of the volcano, which controls edifice size and
772 magma supply [Borgia et al., 2000]. Volcanoes underlain by thick, weak layers and that have
773 high magma supply rates or that are very large are more prone to the development of persistent
774 flank instability compared to volcanoes lacking one or more of these elements. Plotting
775 volcanoes in the two-dimensional space defined by magmatic activity and structural setting
776 demonstrates that a distinction can be drawn between volcanoes with persistent flank instability
777 and those without (Fig. 8). Such a plot is inherently schematic in nature, owing to the fact that
778 edifice size and magma supply are somewhat independent (for instance, El Hierro is larger in
779 volume than Piton de la Fournaise, yet has a lower magma supply), but is nonetheless illustrative
780 of overall patterns in the characteristics of persistent flank motion. Hawai‘i defines an extreme in
781 this spectrum—old, sediment-covered substrate and large edifices fed by high magma supply—
782 so it is not surprising that flank instability is so intense there. The high rates of flank deformation
783 in Hawai‘i are driven in large part by gravitational spreading (with secondary magmatic forcing)
784 due to the extreme size of the edifices and dense cumulates at the cores of the volcanoes [Clague
785 and Denlinger, 1994; Brooks et al., 2008; Montgomery-Brown et al., 2010, 2015; Plattner et al.,
786 2013]. Piton de la Fournaise and Etna also sit on weak layers of some sort and have relatively
787 high magma supply, but not to the extreme of Kīlauea and Mauna Loa, so the volcanoes are
788 smaller, and flank slip occurs at a lower rate and is influenced to a greater extent by magmatism.
789 Cumbre Vieja instability must be driven by gravitational spreading, given the lack of recent
790 magmatic activity (its most recent eruption was in 1971 [González et al., 2010]) and its relatively
791 large volume. The rate of flank motion (a few mm/yr) is smaller than that recorded at Etna and
792 Piton de la Fournaise (a few cm/yr); however, flank motion rates might change drastically during
793 an episode of magmatic unrest, by analogy with Piton de la Fournaise and Etna. Even though
794 some Galápagos volcanoes, like Sierra Negra, have magma supply rates comparable to that of
795 Piton de la Fournaise (Fig. 7) [Poland, 2014a], the volcanoes are relatively small and sitting on
796 young ocean floor with little sedimentary cover, and therefore not prone to persistent flank
797 motion (Fig. 8).

798 Since Cumbre Vieja shows signs of persistent instability, shouldn’t other volcanoes in the
799 Canary Islands, which have similar geologic settings, sizes, and magmatic activity, also be
800 characterized by creeping flanks? It is possible that such deformation is occurring but has yet to

801 be detected because it is so small. Indeed, Tenerife is subsiding by a few mm/yr, likely due to
802 gravitational loading of weak lithosphere [Fernández et al., 2009]. La Palma and El Hierro, being
803 the most westward of the Canary Islands, are unbuttressed to the west and, therefore, are a
804 logical place to look for flank motion. El Hierro has experienced multiple catastrophic collapses
805 [Holcomb and Searle, 1991; Masson et al., 2002], so its subaerial flanks are small and may not
806 be deforming at this time (although one might speculate that they were moving persistently prior
807 to their collapse, which might also have been the case at Fogo—a volcano of similar volume and
808 eruptive activity and also sitting on old ocean floor). It is also possible that low and
809 discontinuous magma supply to volcanoes like Fogo and El Hierro may obscure manifestation of
810 persistent creep-like instability. Volcanoes exemplified by Cumbre Vieja, El Hierro, and Fogo
811 therefore appear to lie at the boundary between the presence and absence of persistent flank
812 motion; flank creep may occur, but at very low deformation rates that are difficult to detect.

813 The framework of magmatic activity versus structural setting may also explain the style
814 of flank faulting. High magma supply, a large edifice volume, and a subvolcanic weak layer can
815 result in a heavily faulted flank, as is the case at Etna, Kīlauea, and Mauna Loa. Piton de la
816 Fournaise has comparatively lower magma supply, is smaller in volume, and may have a less-
817 developed weak layer, and so the flank has not been heavily faulted. Cumbre Vieja is a relatively
818 large edifice and is underlain by thick oceanic sediments (based on the age of the sea floor), but a
819 lack of strong magmatic activity may not be conducive to flank faulting.

820

821 **5. Conclusions**

822 Although Kīlauea, Piton de la Fournaise, and Etna are each characterized by persistent
823 flank motion, the manifestations and mechanisms of the process at the three volcanoes cover a
824 wide range. At Kīlauea, persistent instability is driven mostly by gravitational spreading of
825 magmatic cumulates and accommodated along a detachment fault at 8–10 km depth, and the
826 flank is heavily faulted (though the faults may only rupture during strong earthquakes). At Etna
827 and Piton de la Fournaise, flank motion is driven to a greater extent by magmatism, and the plane
828 along which motion occurs is poorly known but probably within a few km of the surface. Etna’s
829 flank is heavily faulted with blocks that move independently, while the flank of Piton de la
830 Fournaise shows no obvious signs of faulting.

831 The similarities and differences in flank motion at the three volcanoes can be expressed
832 in terms of the volcano’s structural setting and its level of magmatic activity. Volcanoes that
833 grow to great size, presumably due to high rates of magma supply and/or long durations of
834 activity, can develop instabilities that are governed by gravitational spreading. Flank motion at
835 smaller volcanoes but that also have frequent eruptions and intrusions may be more highly
836 influenced by magmatism, which may in turn be related to the extent of flank faulting (higher at
837 Etna, which is supplied by a greater rate of magma supply compared to Piton de la Fournaise). In
838 all cases, a subhorizontal plane of weakness of some sort is a necessary component for persistent
839 flank instability; volcanoes lacking such a weak layer, like those of the Galápagos, show no signs
840 of long-term flank motion (though catastrophic flank collapse may still occur). An unbuttressed
841 flank may also be a requirement for accommodating flank slip, although such a condition is not
842 strictly required (as demonstrated by Mauna Loa), nor is it a specific trigger for persistent
843 instability.

844 We suggest that the framework of magmatic activity versus structural setting may be a
845 useful starting point for understanding the spectrum of potential long-term persistent flank
846 instability at large basaltic volcanoes around the world—why sliding flanks are common in some
847 places but absent in others, and how sliding flanks vary from volcano to volcano. Such a
848 framework provides a convenient, if subjective, means of understanding this complex process,
849 evaluating its importance, and interpreting its surface expression at volcanoes that may be less
850 well understood than our three example edifices. Further, the proposed conceptual model is a
851 good alternative to the use of any one specific volcano as an analog. Kīlauea is often cited as a
852 “type example” for flank instability, thanks to the long history of study and, by association, more
853 developed understanding of the process, but the example is an extreme one that does not
854 necessarily translate well to other volcanoes (except, perhaps, Mauna Loa, which is similar in
855 size, setting, and magmatic activity).

856 We also hope that our proposed framework can serve as a starting point for volcanoes
857 that experience catastrophic collapse. While infrequent, large landslides represent a potentially
858 devastating hazard, and the conditions of their occurrence are poorly understood. Perhaps the
859 most poignant question is whether or not flanks characterized by persistent long-term motion
860 will eventually collapse catastrophically. By connecting future models of flank collapse with the

861 framework we have proposed here, it may be possible to develop a better overall understanding
862 of all forms of flank instability.

863

864 **Acknowledgments**

865

866 Funding for this work was provided by the U.S. Geological Survey, by Agence Nationale de la
867 Recherche under contract ANR-16-CE04-0004-01 (SlideVOLC), and by the European
868 MEDSUV project. We are grateful for helpful comments from Dan Dzurisin, and thorough
869 reviews by Ingrid Johanson, Bill Chadwick, and Valerio Acocella. This is IGP contribution
870 n°XXXX.

871

872 **Figure Captions**

873

874 Figure 1. Map showing locations of large basaltic volcanoes discussed in the text.

875

876 Figure 2. Shaded relief map of Kīlauea Volcano, Hawaii, showing major structural features
877 discussed in the text.

878

879 Figure 3. Shaded relief map of Piton de la Fournaise volcano, La Réunion, showing major
880 structural features discussed in the text.

881

882 Figure 4. Shaded relief map of Etna volcano, Sicily, showing major structural features discussed
883 in the text. TL: Tindari-Letojanni fault; ME: Malta Escarpment; CG: Catania-Gela foredeep.

884

885 Figure 5. Flank displacements determined from GNSS at (A) Kīlauea, (B) Piton de la Fournaise,
886 and (C) Etna. Time periods shown correspond to periods of steady eruptive activity and summit
887 subsidence at Kīlauea (1997–2002), of magmatic quiescence at Piton de la Fournaise (2012–
888 2013) and of summit eruptions at Etna (2012–2016).

889

890 Figure 6. Time series of flank displacement at Kīlauea (red), Etna (blue), and Piton de la
891 Fournaise (black) at the GNSS station located closest to the coastlines at each volcano. Offsets in

892 the Kīlauea time series are a result of an East Rift Zone fissure eruption in 2011 and slow slip
893 events (SSEs) in 2012 and 2015.

894

895 Figure 7. Plots showing relations between magma supply (top) and edifice size (bottom) versus
896 the maximum rate of horizontal flank motion. Values are from Table 1, Schmincke [1982],
897 González et al. [2010; 2013], Poland [2014a], and Bagnardi et al. [2016]. Volcanoes of the
898 Canary and Galápagos archipelagos are grouped, given their internal similarities in size and
899 magma supply. Red labels indicate volcanoes with persistent flank motion (in the case of the
900 Canary Islands, only Cumbre Vieja is known to have a persistently moving flank).

901

902 Figure 8. Conceptual framework for understanding persistent long-term flank instability. X-axis
903 defines magma supply and/or edifice size (noting that a large edifice is possible under conditions
904 of low magma supply if plate velocity is low) increasing to the right, and Y-axis is structural
905 setting, increasing in thickness of weak substrate upward. Rates of flank motion increase with
906 magmatic activity and structural setting, with gravitational spreading being the dominant driving
907 mechanism at larger volcanoes, and flank faulting important where magma supply is highest.

908

909

910 **Table 1.** Comparison of the general characteristics of Kīlauea, Piton de la Fournaise, and Etna volcanoes.
 911 Numbers in brackets give references for specific characteristics.
 912

Characteristic	Kīlauea	Piton de la Fournaise	Etna
Volume	31,600–11,000 km ³ [1,2]	~1500 km ³ [3]	~684 km ³ [4]
Plate tectonic setting	Intraplate; 10 cm/yr plate velocity [5]	Intraplate; 2 cm/yr plate velocity [5]	Plate boundary (convergent)
Age	~275 ka (inception), ~100 ka (shield) [1]	~500 ka [6]	~500 ka (tholeiitic), ~200 ka (basaltic) [7]
Magma supply	~0.1 km ³ /yr [8]	0.01–0.04 km ³ /yr [9,10]	~0.075 km ³ /yr [11]
Detachment	Yes, between volcanic pile and ocean floor; many earthquakes	No clear evidence, possible sill or along interface with Piton des Neiges; some earthquakes 1-2 km b.s.l.	No clear evidence, possible in the sedimentary basement; no earthquakes along possible detachment
Flank faulting	Normal faults parallel to coast; no clear evidence of motion except during large earthquakes	No apparent flank faulting	Normal and strike-slip faults, azimuths linked to regional tectonic setting and dynamics to volcanic activity
Horizontal displ. from flank instability	Velocity increases to the coast; max ~8 cm/yr [12]	Velocity is similar at different elevations during rest periods; ~1.4 cm/yr [13]	Velocity increases to the coast; max 3–5 cm/yr [14,15]
Vertical displ. from flank instability	Uplift along the coast	Subsidence, mostly due to compaction of recent lava flows	Subsidence along the coast (eastward of the Timpe faults)
Interaction with summit magmatism	Not obvious	Increased flank motion during summit inflation	Increased flank motion during summit inflation
Interaction with flank/rift magmatism	Intrusions encouraged by flank motion; slow slip events promote and are promoted by rift zone eruptions and intrusions	Strong flank motion associated with distal eruptions; relaxation time of months–years	Strong flank motion due to rift zone intrusions and eruptions; relaxation time of months–years

913
 914 [1] Lipman and Calvert, 2013
 915 [2] Robinson and Eakins, 2006
 916 [3] Villeneuve et al., 2014
 917 [4] Bisson et al., 2016
 918 [5] Gripp and Gordon, 2002
 919 [6] Gillot and Nativel, 1989
 920 [7] Branca et al., 2011
 921 [8] Poland et al., 2014
 922 [9] White, 1993
 [10] Peltier et al., 2009
 [11] Allard et al., 2006
 [12] Owen et al., 2000a
 [13] Peltier et al., 2015b
 [14] Solaro et al., 2010
 [15] Bonforte et al., 2011

923 **References**

- 924 Acocella, V., Behncke, B., Neri, M. and D'Amico, S., 2003. Link between major flank slip and
 925 2002–2003 eruption at Mt. Etna (Italy). *Geophys. Res. Lett.*, 30(24):
 926 doi:10.1029/2003GL018642.
- 927 Acocella, V., Neri, M., Behncke, B., Bonforte, A., Del Negro, C., Ganci, G., 2016. Why Does a
 928 Mature Volcano Need New Vents? The Case of the New Southeast Crater at Etna. *Front.*
 929 *Earth Sci.*, 4: 67, doi:10.3389/feart.2016.00067.
- 930 Allard, P., Behncke, B., D'Amico, S., Neri, M., Gambino, S., 2006. Mount Etna 1993–2005:
 931 Anatomy of an evolving eruptive cycle. *Earth Sci. Rev.*, 78(1–2): 84–114,
 932 doi:10.1016/j.earscirev.2006.04.002.
- 933 Alparone, S., Barberi, G., Bonforte, A., Maiolino, V., Ursino, U., 2011. Evidence of multiple
 934 strain fields beneath the eastern flank of Mt. Etna volcano (Sicily, Italy) deduced from
 935 seismic and geodetic data during 2003–2004. *Bull. Volcanol.*, 73(7): 869–885,
 936 doi:10.1007/s00445-011-0456-1.
- 937 Alparone, S., Bonaccorso, A., Bonforte, A., Currenti, G., 2013. Long-term stress-strain analysis
 938 of volcano flank instability: The eastern sector of Etna from 1980 to 2012. *J. Geophys.*
 939 *Res.*, 118(9): doi:10.1002/jgrb.50364.
- 940 Amelung, F. and Day, S., 2002. InSAR observations of the 1995 Fogo, Cape Verde, eruption:
 941 Implications for the effects of collapse events upon island volcanoes. *Geophys. Res. Lett.*,
 942 29(12): doi:10.129/2001GL013760.
- 943 Anderson, K.R., and Poland, M.P., 2016. Bayesian estimation of magma supply, storage, and
 944 eruption rates using a multiphysical volcano model: Kīlauea Volcano, 2000–2012. *Earth*
 945 *Planet. Sci. Lett.*, 447: 161–171, doi: 10.1016/j.epsl.2016.04.029.
- 946 Azzaro, R., 2004. Seismicity and active tectonic in the Etna region: constrain for seismotectonic
 947 model. In: Bonaccorso A., Calvari S., Coltelli M., Del Negro C., Falsaperla S. (Eds.), *Mt.*
 948 *Etna Volcano Laboratory. Am. Geoph. Union Geophys. Mono.*, 143, pp. 205–220,
 949 doi:10.1029/143GM13.
- 950 Azzaro, R., Bonforte, A., Branca, S., Guglielmino, F., 2013. Geometry and kinematics of the
 951 fault systems controlling the unstable flank of Etna volcano (Sicily). *J. Volcanol.*
 952 *Geotherm. Res.* 251: 5–15, doi: 10.1016/j.jvolgeores.2012.10.001.
- 953 Bachèlery, P., 1981. Le Piton de la Fournaise (Ile de La Réunion). *Etude volcanologique,*
 954 *structural et pétrologique. PhD Thesis, Univ. Clermont-Ferrand II, 215 p.*
- 955 Bagnardi, M., González, P.J. and Hooper, A., 2016. High-resolution digital elevation model from
 956 tri-stereo Pleiades-1 satellite imagery for lava flow volume estimates at Fogo Volcano.
 957 *Geophys. Res. Lett.*, 43(12): 6267–6275, doi:10.1002/2016GL069457.
- 958 Barreca, G., Bonforte, A., Neri, M., 2013. A pilot GIS database of active faults of Mt. Etna
 959 (Sicily): A tool for integrated hazard evaluation. *J. Volcanol. Geotherm. Res.* 251: 170–
 960 186, doi:10.1016/j.jvolgeores.2012.08.013.
- 961 Battaglia, J., Ferrazzini, V., Staudacher, T., Aki, K., Cheminée, J.L., 2005. Pre-eruptive
 962 migration of earthquakes at the Piton de La Fournaise volcano (Réunion Island). *Geophys.*
 963 *J. Int.* 161(2): 549–558, doi:10.1111/j.1365-246X.2005.02606.x.
- 964 Ben-Avraham, Z., Grasso, M., 1991. Crustal structure variations and transcurrent faulting at the
 965 eastern and western margins of the eastern Mediterranean. *Tectonophys.*, 75(3–4): 269–
 966 277, doi:10.1016/0040-1951(91)90326-N.
- 967 Billi, A., Acocella, V., Funiciello, R., Giordano, G., Lanzafame, G. and Neri, M., 2003.
 968 Mechanisms for ground-surface fracturing and incipient slope failure associated with the

- 969 2001 eruption of Mt. Etna, Italy: Analysis of ephemeral field data. *J. Volcanol. Geotherm.*
970 *Res.*, 122(3): 281–294, doi:10.1016/S0377-0273(02)00507-3.
- 971 Bisson, M., Spinetti, C., Neri, M. and Bonforte, A., 2016. Mt. Etna volcano high-resolution
972 topography: Airborne LiDAR modelling validated by GPS data. *Int. J. Digital Earth*, 9(7):
973 710–732, doi:10.1080/17538947.2015.1119208.
- 974 Bonaccorso, A., Bonforte, A., Guglielmino, F., Palano, M., Puglisi G., 2006. Composite ground
975 deformation pattern forerunning the 2004–2005 Mount Etna eruption. *J. Geophys. Res.*,
976 111(B12): doi:10.1029/2005jb004206.
- 977 Bonaccorso, A., Bonforte, A., Gambino, S., Mattia, M., Guglielmino, F., Puglisi, G., Boschi, E.,
978 2009. Insight on recent Stromboli eruption inferred from terrestrial and satellite ground
979 deformation measurements. *J. Volcanol. Geotherm. Res.*, 182(3–4): 172–181,
980 doi:10.1016/j.jvolgeores.2009.01.007.
- 981 Bonaccorso, A., Bonforte, A., Currenti, G., Del Negro, C., Di Stefano, A., Greco, F., 2011.
982 Magma storage, eruptive activity and flank instability: Inferences from ground deformation
983 and gravity changes during the 1993–2000 recharging of Mt. Etna volcano. *J. Volcanol.*
984 *Geotherm. Res.*, 200(3–4): 245–254, doi:10.1016/j.jvolgeores.2011.01.001.
- 985 Bonali, F., Corazzato, C., Tibaldi, A., 2011. Identifying rift zones on volcanoes: An example
986 from La Réunion Island, Indian Ocean. *Bull. Volcanol.* 73(3): 347–366,
987 doi:10.1007/s00445-010-0416-1.
- 988 Bonforte, A., Puglisi, G., 2003. Magma uprising and flank dynamics on Mount Etna volcano,
989 studied using GPS data (1994–1995). *J. Geophys. Res.*, 108(B3), 2153:
990 doi:10.1029/2002JB001845.
- 991 Bonforte, A., Puglisi, G., 2006. Dynamics of the eastern flank of Mt. Etna volcano (Italy)
992 investigated by a dense GPS network. *J. Volcanol. Geotherm. Res.*, 153(3–4): 357–369,
993 doi:10.1016/j.jvolgeores.2005.12.005.
- 994 Bonforte, A., Guglielmino, F., 2015. Very shallow dyke intrusion and potential slope failure
995 imaged by ground deformation: The 28 December 2014 eruption on Mount Etna. *Geophys.*
996 *Res. Lett.*, 42(8): 2727–2733, doi:10.1002/2015GL063462.
- 997 Bonforte, A., Branca, S., Palano, M., 2007a. Geometric and kinematic variations along the active
998 Pernicana fault: Implication for the dynamics of Mount Etna NE flank (Italy). *J. Volcanol.*
999 *Geotherm. Res.*, 160(1–2): 210–222, doi:10.1016/j.jvolgeores.2006.08.009.
- 1000 Bonforte, A., Carbone, D., Greco, F., Palano, M., 2007b. Intrusive mechanism of the 2002 NE-
1001 rift eruption at Mt Etna (Italy) modelled using GPS and gravity data. *Geophys. J. Int.*,
1002 169(1): 339–347, doi:10.1111/j.1365-246X.2006.03249.x.
- 1003 Bonforte A., Bonaccorso, A., Guglielmino, F., Palano, M., Puglisi, G., 2008. Feeding system and
1004 magma storage beneath Mt. Etna as revealed by recent inflation/deflation cycles. *J.*
1005 *Geophys. Res.* 113(5): doi:10.1029/2007JB005334.
- 1006 Bonforte, A., Gambino, S., Neri, M., 2009. Intrusion of eccentric dikes: The case of the 2001
1007 eruption and its role in the dynamics of Mt. Etna volcano. *Tectonophysics.*, 471(1–2): 78–86,
1008 doi:10.1016/j.tecto.2008.09.028.
- 1009 Bonforte, A., Guglielmino, F., Coltelli, M., Ferretti, A., Puglisi, G., 2011. Structural assessment
1010 of Mount Etna volcano from Permanent Scatterers analysis, *Geochem. Geophys. Geosyst.*,
1011 12(2): doi:10.1029/2010GC003213.
- 1012 Bonforte, A., Carnazzo, A., Gambino, S., Obrizzo, F., Puglisi, G., 2013a. A multidisciplinary
1013 study of an active fault crossing urban areas: The Trecastagni Fault at Mt. Etna (Italy). *J.*
1014 *Volcanol. Geotherm. Res.*, 251: 41–49, doi:10.1016/j.jvolgeores.2012.05.001.

- 1015 Bonforte, A., Federico, C., Giammanco, S., Guglielmino, F., Liuzzo, M., Neri, M., 2013b. Soil
1016 gases and SAR measurements reveal hidden faults on the sliding flank of Mt. Etna (Italy).
1017 *J. Volcanol. Geotherm. Res.*, 251: 27–40, doi:10.1016/j.jvolgeores.2012.08.010.
- 1018 Bonforte, A., Guglielmino, F., Puglisi, G., 2013c. Interaction between magma intrusion and flank
1019 dynamics at Mt. Etna in 2008, imaged by integrated dense GPS and DInSAR data.
1020 *Geochem. Geophys. Geosyst.*, 14(8): 2818–2835, doi:10.1002/ggge.20190.
- 1021 Bonforte, A., Gonzalez, P.J., Fernandez, J., 2016. Joint Terrestrial and Aerial Measurements to
1022 Study Ground Deformation: Application to the Sciara Del Fuoco at the Stromboli Volcano
1023 (Sicily). *Rem. Sens.*, 8(6): 463, doi:10.3390/rs8060463.
- 1024 Borgia, A., Ferrari, L. and Pasquarè, G., 1992. Importance of gravitational spreading in the
1025 tectonic and volcanic evolution of Mount Etna. *Nature*, 357(6375): 231–235,
1026 doi:10.1038/357231a0.
- 1027 Borgia, A., Delaney, P.T. and Denlinger, R.P., 2000. Spreading Volcanoes. *Ann. Rev. Earth
1028 Planet. Sci.*, 28: 539–570, doi:10.1146/annurev.earth.28.1.539.
- 1029 Branca, S., Del Carlo, P., 2004. Eruptions of Mt. Etna during the past 3,200 years: A revised
1030 compilation integrating the historical and stratigraphic records. In: Bonaccorso A., Calvari
1031 S., Coltelli M., Del Negro C., Falsaperla S. (Eds.), *Mt. Etna Volcano Laboratory*. Am.
1032 *Geoph. Union Geophys. Mono.*, 143, pp. 1–27, doi:10.1029/143GM02.
- 1033 Branca, S., Coltelli, M., Groppelli, G., Lentini, F., 2011. Geological map of Etna volcano,
1034 1:50,000 scale. *Ital. J. Geosci.* 130(3): 265–291, doi: 10.3301/IJG.2011.15.
- 1035 Brenguier, F., Kowalski, P., Staudacher, T., Ferrazzini, V., Lauret, F., Boissier, P., Catherine, P.,
1036 Lemarchand, A., Pequegnat, C., Meric, O., Pardo, C., Peltier, A., Tait, T., Shapiro, N.M.,
1037 Campillo, M., Di Muro, A., 2012. First results from the UnderVolc high resolution seismic
1038 and GPS network deployed on Piton de la Fournaise volcano. *Seismol. Res. Lett.* 83(7):
1039 97–102, doi:10.1785/gssrl.83.1.97.
- 1040 Brooks, B.A., Foster, J.H., Bevis, M., Frazer, L.N., Wolfe, C.J. and Behn, M., 2006. Periodic
1041 slow earthquakes on the flank of Kilauea volcano, Hawaii. *Earth Planet. Sci. Lett.*, 246(3–4):
1042 207–216, doi:10.1016/j.epsl.2006.03.035.
- 1043 Brooks, B.A., Foster, J., Sandwell, D., Wolfe, C.J., Okubo, P., Poland, M. and Myer, D., 2008.
1044 Magmatically triggered slow slip at Kilauea Volcano, Hawaii. *Science*, 321(5893): 1177,
1045 doi:10.1126/science.1159007.
- 1046 Calvari, S., Tanner, L.H., Groppelli, G., Norini, G., 2004. Valle del Bove, Eastern Flank of Etna
1047 volcano: A comprehensive model for the opening of the depression and implications for
1048 future hazards. In: Bonaccorso A., Calvari S., Coltelli M., Del Negro C., Falsaperla S.
1049 (Eds.), *Mt. Etna Volcano Laboratory*. Am. *Geoph. Union Geophys. Mono.*, 143, pp. 65–75,
1050 doi:10.1029/143GM05.
- 1051 Cannon, E.C. and Bürgmann, R., 2001. Prehistoric fault offsets of the Hilina fault system, south
1052 flank of Kilauea Volcano, Hawaii. *J. Geophys. Res.*, 106(B3): 4207–4219,
1053 doi:10.1029/2000JB900412.
- 1054 Cannon, E.C., Bürgmann, R. and Owen, S.E., 2001. Shallow normal faulting and block rotation
1055 associated with the 1975 Kalapana earthquake, Kilauea Volcano, Hawaii. *Bull. Seismol. Soc.
1056 Am.*, 91(6): 1553–1562, doi:10.1785/0120000072.
- 1057 Carracedo, J.C., 1999. Growth, structure, instability and collapse of Canarian volcanoes and
1058 comparisons with Hawaiian volcanoes. *J. Volcanol. Geotherm. Res.*, 94(1): 1–19,
1059 doi:10.1016/S0377-0273(99)00095-5.

1060 Carracedo, J.C., Day, S.J., Guillou, H., Torrado, F.J.P., 1999. Giant quaternary landslides in the
1061 evolution of La Palma and El Hierro, Canary Islands. *J. Volcanol. Geotherm. Res.*, 94(1):
1062 169–190, doi:10.1016/S0377-0273(99)00102-X.

1063 Cayol, V., Catry, T., Michon, L., Chaput, M., Famin, V., Bodart, O., Froger, J.-L. and
1064 Romagnoli, C., 2014. Sheared sheet intrusions as a mechanism for lateral flank displacement
1065 on basaltic volcanoes: Applications to Réunion Island volcanoes. *J. Geophys. Res.*, 119(10):
1066 7607–7635, doi:10.1002/2014JB011139.

1067 Cervelli, P., Segall, P., Johnson, K., Lisowski, M. and Miklius, A., 2002a. Sudden aseismic fault
1068 slip on the south flank of Kilauea volcano. *Nature*, 415(6875): 1014-1018,
1069 doi:10.1038/4151014a.

1070 Cervelli, P., Segall, P., Amelung, F., H., G., Owen, S., Miklius, A. and Lisowski, M., 2002b. The
1071 12 September 1999 Upper East Rift Zone dike intrusion at Kilauea Volcano, Hawaii. *J.*
1072 *Geophys. Res.*, 107(B7): doi:10.1029/2001JB000602.

1073 Chadwick, W.W., Jr. and Dieterich, J.H., 1995. Mechanical modeling of circumferential and
1074 radial dike intrusion on Galapagos volcanoes. *J. Volcanol. Geotherm. Res.*, 66(1–4): 37–52,
1075 doi:10.1016/0377-0273(94)00060-T.

1076 Chaput, M., Pinel, V., Famin, V., Michon, L., Froger, J.-L., 2014, Cointrusive shear
1077 displacement by sill intrusion in a detachment: A numerical approach. *Geophys. Res. Lett.*,
1078 41(6): 1937–1943, doi:10.1002/2013GL058813.

1079 Chen, Y., Remy, D., Froger, J.-L., Peltier, A., Villeneuve, N., Darrozes, J., Perfettini, H.,
1080 Bonvalot, S., in revision. Long-term ground displacement observed by InSAR and GNSS
1081 at Piton de la Fournaise volcano between 2009 and 2014. *Rem. Sens. Environ.*

1082 Chiocci, F.L., Coltelli, M., Bosman, A., Cavallaro, D., 2011. Continental margin large-scale
1083 instability controlling the flank sliding of Etna volcano. *Earth Planet. Sci. Lett.*, 305(1–2):
1084 57–64, doi:10.1016/j.epsl.2011.02.040.

1085 Clague, D.A., and Dalrymple, G.B., 1987. The Hawaiian-Emperor volcanic chain; part 1.
1086 Geologic evolution. In: Decker, R.W., Wright, T.L., Stauffer, P.H. (Eds.), *Volcanism in*
1087 *Hawaii*. U.S. Geol. Surv. Prof. Pap., 1350, pp. 5–54.

1088 Clague, D.A. and Denlinger, R.P., 1994. Role of olivine cumulates in destabilizing the flanks of
1089 Hawaiian volcanoes. *Bull. Volcanol.*, 56(6–7): 425–434, doi:10.1007/BF00302824.

1090 Clague, D.A. and Sherrod, D.R., 2014. Growth and degradation of Hawaiian Volcanoes. In:
1091 Poland, M.P., Landowski, C.M., Takahashi, T.J. (Eds.), *Characteristics of Hawaiian*
1092 *Volcanoes*. U.S. Geol. Surv. Prof. Pap., 1801, pp. 97–146, doi:10.3133/pp18013.

1093 Clarke, D., Brenguier, F., Froger, J.-L., Shapiro, N.M., Peltier, A., Staudacher, T., 2013. Timing
1094 of a large volcanic flank movement at Piton de la Fournaise Volcano using noise-based
1095 seismic monitoring and ground deformation measurements. *Geophys. J. Int.*, 195(2): 1132–
1096 1140, doi:10.1093/gji/ggt276.

1097 Courteaud, M., 1996. Etude des structures géologiques et hydrogéologiques du massif de la
1098 Fournaise par la méthode audiomagnétotellurique. Ph.D. Dissertation, Université de la
1099 Réunion, 212 pp.

1100 Day, S.J., Da Silva, S.H. and Fonseca, J.F.B.D., 1999. A past giant lateral collapse and present-
1101 day flank instability of Fogo, Cape Verde Islands. *J. Volcanol. Geotherm. Res.*, 94(1): 191–
1102 218, doi:10.1016/S0377-0273(99)00103-1.

1103 De Gori, P., Chiarabba, C., Patanè, D., 2005. Qp structure of Mount Etna: Constraints for the
1104 physics of the plumbing system. *J. Geophys. Res.*, 110(5): doi:10.1029/2003JB002875.

1105 Del Carlo, P., Vezzoli, L., Coltelli, M., 2004. Last 100 ka Tephrostratigraphic record of Mount

1106 Etna. In: Bonaccorso A., Calvari S., Coltelli M., Del Negro C., Falsaperla S. (Eds.), Mt.
1107 Etna Volcano Laboratory. Am. Geoph. Union Geophys. Mono., 143, pp. 77–89,
1108 doi:10.1029/143GM06.

1109 Delaney, P.T., Fiske, R.S., Miklius, A., Okamura, A.T. and Sako, M.K., 1990. Deep magma
1110 body beneath the summit and rift zones of Kilauea Volcano, Hawaii. *Science*, 247(4948):
1111 1311–1316, doi:10.1126/science.247.4948.1311.

1112 Denlinger, R.P. and Morgan, J.K., 2014. Instability of Hawaiian Volcanoes. In: Poland, M.P.,
1113 Landowski, C.M., Takahashi, T.J. (Eds.), *Characteristics of Hawaiian Volcanoes*. U.S. Geol.
1114 Surv. Prof. Pap., 1801, pp. 149–176, doi:10.3133/pp18014.

1115 Derrien, A., Villeneuve, N., Peltier, A., Beauducel, F., 2015. Retrieving 65 years of volcano
1116 summit deformation from multitemporal structure from motion: The case of Piton de la
1117 Fournaise (La Réunion Island). *Geophys. Res. Lett.* 42(17): 6959–6966,
1118 doi:10.1002/2015GL064820.

1119 Di Muro, A., Métrich, N., Vergani, D., Rosi, M., Armienti, P., Fougeroux, T., Deloule, E.,
1120 Arienzo, I., Civetta, L., 2014. The Shallow Plumbing System of Piton de la
1121 Fournaise Volcano (La Réunion Island, Indian Ocean) Revealed by the Major 2007
1122 Caldera-Forming Eruption. *J Petrol.* 55(7): 1287–1315, doi:10.1093/petrology/egu025.

1123 Di Traglia, F., Intrieri, E., Nolesini, T., Bardi, F., Del Ventisette, C., Ferrigno, F., Frangioni, S.,
1124 Frodella, W., Gigli, G., Lotti, A., Tacconi Stefanelli, C., Tanteri, L., Leva, D., Casagli, N.,
1125 2014. The ground-based InSAR monitoring system at Stromboli volcano: linking changes
1126 in displacement rate and intensity of persistent volcanic activity. *Bull. Volcanol.*, 76: 786,
1127 doi:10.1007/s00445-013-0786-2.

1128 Dieterich, J.H., 1988. Growth and persistence of Hawaiian volcanic rift zones. *J. Geophys. Res.*,
1129 93(B5): 4258–4270, doi:10.1029/JB093iB05p04258.

1130 Duffield, W.A., 1975. Structure and Origin of the Koa'e Fault System, Kilauea Volcano, Hawaii.
1131 U.S. Geol. Surv. Prof. Pap., 856, 12 pp.

1132 Duncan, R. A., 1981. Hotspots in the southern oceans: An absolute frame of reference for motion
1133 of the Gondwana continents. *Tectonophys.* 74(1–2): 29–24, doi:10.1016/0040-
1134 1951(81)90126-8.

1135 Dzurisin, D., Anderson, L.A., Eaton, G.P., Koyanagi, R.Y., Lipman, P.W., Lockwood, J.P.,
1136 Okamura, R.T., Puniwai, G.S., Sako, M.K. and Yamashita, K.M., 1980. Geophysical
1137 observations of Kilauea Volcano, Hawaii; 2, Constraints on the magma supply during
1138 November 1975-September 1977. *J. Volcanol. Geotherm. Res.*, 7(3–4): 241–269,
1139 doi:10.1016/0377-0273(80)90032-3.

1140 Famin, V. and Michon, L., 2010. Volcano destabilization by magma injections in a detachment.
1141 *Geology*, 38(3): 219–222, doi:10.1130/G30717.1.

1142 Fernández, J., Tizzani, P., Manzo, M., Borgia, A., González, P.J., Martí, J., Pepe, A., Camacho,
1143 A.G., Casu, F., Berardino, P., Prieto, J.F. and Lanari, R., 2009. Gravity-driven deformation
1144 of Tenerife measured by InSAR time series analysis. *Geophys. Res. Lett.*, 36(4):
1145 doi:10.1029/2008GL036920.

1146 Froger, J.L., Merle, O., Briole, P., 2001. Active spreading and regional extension at Mount Etna
1147 imaged by SAR interferometry. *Earth Planet. Sci. Lett.*, 187(3): 245–258,
1148 doi:10.1016/S0012-821X(01)00290-4.

1149 Froger, J.-L., Famin, V., Cayol, V., Augier, A., Michon, L., Lénat, J.-L., 2015. Time-dependent
1150 displacements during and after the April 2007 eruption of Piton de la Fournaise, revealed
1151 by interferometric data. *J. Volcanol. Geotherm. Res.* 296: 55–68,

1152 doi:10.1016/j.jvolgeores.2015.02.014.

1153 Gailler, L.-S, Lénat, J.-F., Lambert, M., Levieux, G., Villeneuve, N., Froger, J.-L., 2009. Gravity
1154 structure of Piton de la Fournaise volcano and inferred mass transfer during the 2007 crisis.
1155 J. Volcanol. Geotherm. Res. 184(1–2): 31–48, doi:10.1016/j.jvolgeores.2009.01.024.

1156 Gambino, S., Bonforte A., Carnazzo A., Falzone G., Ferrari F., Ferro, A., Guglielmino F.,
1157 Laudani G., Maiolino, V., Puglisi G., 2011. Displacement across the Trecastagni Fault (Mt.
1158 Etna) and induced seismicity: The October 2009 to January 2010 episode. Ann. Geophys.,
1159 54(4): doi: 10.4401/ag-4841.

1160 Geist, D., White, W.M., Albarede, F., Harpp, K., Reynolds, R., Blichert-Toft, J. and Kurz, M.,
1161 2002. Volcanic evolution in the Galapagos: The dissected shield of Volcan Ecuador.
1162 Geochem., Geophys., Geosys., 3(10): doi:10.1029/2002GC000355.

1163 Geist, D., Chadwick, W. and Johnson, D., 2006. Results from new GPS and gravity monitoring
1164 networks at Fernandina and Sierra Negra Volcanoes, Galápagos, 2000–2002. J. Volcanol.
1165 Geotherm. Res., 150(1–3): 79–97, doi:10.1016/j.jvolgeores.2005.07.003.

1166 Gillot, P.- Y., Nativel, P., 1989. Eruption history of the Piton de la Fournaise volcano, Reunion
1167 Island, Indian Ocean. J. Volcanol. Geotherm. Res. 36(1–3): 53–65, doi:10.1016/0377-
1168 0273(89)90005-X.

1169 González, P.J., Tiampo, K.F., Camacho, A.G. and Fernández, J., 2010. Shallow flank
1170 deformation at Cumbre Vieja volcano (Canary Islands): Implications on the stability of steep-
1171 sided volcano flanks at oceanic islands. Earth Planet. Sci. Lett., 297(3–4): 545–557,
1172 doi:10.1016/j.epsl.2010.07.006.

1173 González, P.J., Samsonov, S.V., Pepe, S., Tiampo, K.F., Tizzani, P., Casu, F., Fernández, J.,
1174 Camacho, A.G. and Sansosti, E., 2013. Magma storage and migration associated with the
1175 2011–2012 El Hierro eruption: implications for crustal magmatic systems at oceanic island
1176 volcanoes. J. Geophys. Res., 118(8): 4361–4377, doi:10.1002/jgrb.50289.

1177 González, P.J., Bagnardi, M., Hooper, A.J., Larsen, Y., Marinkovic, P., Samsonov, S.V. and
1178 Wright, T.J., 2015. The 2014-2015 eruption of Fogo volcano: geodetic modelling of
1179 Sentinel-1 TOPS interferometry. Geophysical Research Letters, 42(21): 9239–9246,
1180 doi:10.1002/2015GL066003.

1181 Got., J.-L., and Okubo, P.G., 2003. New insights into Kilauea's volcano dynamics brought by
1182 large-scale relative relocation of microearthquakes. J. Geophys. Res., 108(B7):
1183 doi:10.1029/2002JB002060

1184 Got, J. L., Peltier, A., Staudacher, T., Kowalski, P., Boissier, P., 2013. Edifice strength and
1185 magma transfer modulation at Piton de la Fournaise volcano. J. Geophys. Res., 118(9):
1186 5040–5057, doi:10.1002/jgrb.50350.

1187 Gripp, A.E. and Gordon, R.G., 2002. Young tracks of hotspots and current plate velocities.
1188 Geophys. J. Int., 150(2): 321–361, doi:10.1046/j.1365-246X.2002.01627.x.

1189 Gross, F., Krastel, S., Geersen, J., Behrmann, J.H., Ridente, D., Chiocci, F., Bialas, J., Papenberg,
1190 C., Cukur, D., Urlaub, M., Micallef, A., 2015. The limits of seaward spreading and slope
1191 instability at the continental margin offshore Mt Etna, imaged by high-resolution 2D
1192 seismic data. Tectonophys., 667: 63–76, doi:10.1016/j.tecto.2015.11.011.

1193 Guglielmino, F., Bignami, C., Bonforte, A., Briole, P., Obrizzo, F., Puglisi, G., Stramondo, S.,
1194 Wegmuller U., 2011. Analysis of satellite and in situ ground deformation data integrated
1195 by the SISTEM approach: The April 3, 2010 earthquake along the Pernicana fault (Mt.
1196 Etna - Italy) case study. Earth Planet. Sci. Lett., 312(3–4): 327–336,
1197 doi:10.1016/j.epsl.2011.10.028.

1198 Harris, A. J. L., Steffke, A., Calvari, S., and Spampinato, L., 2011. Thirty years of satellite-
1199 derived lava discharge rates at Etna: Implications for steady volumetric output. *J. Geophys.*
1200 *Res.*, 116(B08): doi:10.1029/2011JB008237.

1201 Harris, A. J. L., Steffke, A., Calvari, S., and Spampinato, L., 2012. Correction to “Thirty years of
1202 satellite-derived lava discharge rates at Etna: Implications for steady volumetric output”. *J.*
1203 *Geophys. Res.*, 117(B08): doi:10.1029/2012JB009431.

1204 Hirn, A., Nicolich, R., Gallart, J., Laigle, M., Cernobori, L., ETNASEIS Scientific Group, 1997.
1205 Roots of Etna volcano in faults of great earthquakes. *Earth Plan. Sci. Lett.* 148(1–2): 171–
1206 191, doi:10.1016/S0012-821X(97)00023-X.

1207 Holcomb, R.T. and Searle, R.C., 1991. Large landslides from oceanic volcanoes. *Marine*
1208 *Geotech.*, 10(1–2): 19–32, doi:10.1080/10641199109379880.

1209 Houliè, N., Briole, P., Bonforte, A., Puiglisi, G., 2006. Large scale ground deformation of Etna
1210 observed by GPS between 1994 and 2001. *Geophys. Res. Lett.*, 33(2):
1211 doi:10.1029/2005GL024414.

1212 Hürlimann, M., Garcia-Piera, J.O., Ledesma, A., 2000. Causes and mobility of large volcanic
1213 landslides: application to Tenerife, Canary Islands. *J. Volcanol. Geotherm. Res.*, 103(1):
1214 121–134, doi:10.1016/S0377-0273(00)00219-5.

1215 Iverson, R.M., 1995. Can magma-injection and groundwater forces cause massive landslides on
1216 Hawaiian volcanoes? *J. Volcanol. Geotherm. Res.*, 66(1–4): 295–308, doi:10.1016/0377-
1217 0273(94)00064-N.

1218 Johnson, J.H., Swanson, D.A., Roman, D.C., Poland, M.P. and Thelen, W.A., 2015. Crustal
1219 stress and structure at Kīlauea Volcano inferred from seismic anisotropy. In: Carey, R.J.,
1220 Cayol, V., Poland, M.P., Weis, D. (Eds.), *Hawaiian Volcanoes, From Source to Surface*. *Am.*
1221 *Geophys. Un. Geophys. Mono.*, 208, pp. 251–268, doi:10.1002/9781118872079.ch12.

1222 Kauahikaua, J. and Miklius, A., 2003. Long-term trends in microgravity at Kilauea's summit
1223 during the Pu`u `O`o-Kupianaha eruption. In: Heliker, C., Swanson, D.A., Takahashi, T.J.
1224 (Eds.), *The Pu`u `O`o-Kupianaha Eruption of Kilauea Volcano, Hawaii: The First 20 Years*,
1225 *U.S. Geol. Surv. Prov. Pap.*, 1676, pp. 165–171.

1226 Krastel, S., Schmincke, H.U., Jacobs, C.L., Rihm, R., Le Bas, T.P. and Alibés, B., 2001.
1227 Submarine landslides around the Canary Islands. *J. Geophys. Res.*, 106(B3): 3977–3997,
1228 doi:10.1029/2000JB900413.

1229 Laigle, M., Hirn, A., Sapin, M., Lépine, J.C., Diaz, J., Gallart, J., Nicolich, R., 2000. Mount Etna
1230 dense array local earthquake P and S tomography and implications for volcanic plumbing.
1231 *J. Geophys. Res.* 105(B9): 21633–21646, doi:10.1029/2000JB900190.

1232 Labazuy, P., 1996. Recurrent landslides events on the submarine flank of Piton de la Fournaise
1233 volcano (Réunion Island). In: McGuire, W.J., Jones, A.P., Neuberg, J. (Eds.), *Volcano*
1234 *Instability on the Earth and Other Planets*. *Geol. Soc. Spec. Publ.*, 110, pp. 293-305.

1235 Le Corvec, N., Walter, T.R., Ruch, J., Bonforte, A., Puglisi, G., 2014. Experimental study of the
1236 interplay between magmatic rift intrusion and flank instability with application to the 2001
1237 Mount Etna eruption. *J. Geophys. Res.*, 119(7): 5356–5368, doi:10.1002/2014JB011224.

1238 Le Friant, A., Lebas, E., Clément, V., Boudon, G., Deplus, C., de Voogd, B., Bachèlery, P.,
1239 2011. A new model for the evolution of la Réunion volcanic complex from complete
1240 marine geophysical surveys. *Geophys. Res. Lett.* 38(9): doi:10.1029/2011GL047489.

1241 Lénat, J.-F., Bachèlery, P., Bonneville, A., Galdéano, A., Labazuy, P., Rousset, D., Vincent, P.,
1242 1990. Structure and morphology of the submarine flank of an active basaltic volcano: Piton
1243 de La Fournaise (Reunion Island, Indian Ocean). *Oceanol. Acta*, 10: 211–223.

1244 Lentini, F., Carbone, S., Guarnieri, P., 2006. Collisional and postcollisional tectonics of the
1245 Apenninic-Maghrebian orogen (southern Italy). In: Dilek, Y., Pavlides, S. (Eds.),
1246 Postcollisional tectonics and magmatism in the Mediterranean region and Asia, Geol. Soc.
1247 Am. Sp. Pap., 409, pp. 57–81, doi:10.1130/2006.2409(04).

1248 Lipman, P.W. and Calvert, A.T., 2013. Modeling volcano growth on the Island of Hawaii: Deep-
1249 water perspectives. *Geosphere*, 9(5): 1348–1383, doi:10.1130/GES00935.1.

1250 Lipman, P.W., Lockwood, J.P., Okamura, R.T., Swanson, D.A. and Yamashita, K.M., 1985.
1251 Ground deformation associated with the 1975 Magnitude-7.2 earthquake and resulting
1252 changes in activity of Kilauea Volcano, Hawaii. U.S. Geol. Surv. Prof. Pap., 1276, 45 pp.

1253 Lundgren, P., Poland, M., Miklius, A., Orr, T., Yun, S.-H., Fielding, E., Liu, Z., Tanaka, A.,
1254 Szeliga, W., Hensley, S. and Owen, S., 2013. Evolution of dike opening during the March
1255 2011 Kamoamoā fissure eruption, Kīlauea Volcano, Hawai‘i. *J. Geophys. Res.*, 118(3): 897–
1256 914, doi:10.1002/jgrb.50108.

1257 Masson, D.G., Watts, A.B., Gee, M.J.R., Urgeles, R., Mitchell, N.C., Le Bas, T.P. and Canals,
1258 M., 2002. Slope failures on the flanks of the western Canary Islands. *Earth Sci. Rev.*, 57(1):
1259 1–35, doi:10.1016/S0012-8252(01)00069-1.

1260 Mathieu, L., Kervyn, M. and Ernst, G.G.J., 2011. Field evidence for flank instability, basal
1261 spreading and volcano-tectonic interactions at Mt Cameroon, West Africa. *Bull. Volcanol.*,
1262 73(7): 851–867, doi:10.1007/s00445-011-0458-z.

1263 Matoza, R.S., Shearer, P.M., Lin, G., Wolfe, C.J. and Okubo, P.G., 2013. Systematic relocation
1264 of seismicity on Hawaii Island from 1992 to 2009 using waveform cross-correlation and
1265 cluster analysis. *J. Geophys. Res.*, 118(5): 2275–2288, doi:10.1002/jgrb.50189.

1266 McGuire, W.J., Moss, J.L., Saunders, S.J., Stewart, I.S., 1996. Dyke induced rifting and edifice
1267 instability at Mount Etna. In: Gravestock, P.J., Mc Guire, W.J. (Eds.), *Etna: Fifteen years*
1268 *on Cheltenham and Gloucester Sp. Publ.*, pp. 20–24.

1269 Merle, O. and Borgia, A., 1996. Scaled experiments of volcanic spreading. *J. Geophys. Res.*,
1270 101(B6): 13,805–13,817, doi:10.1029/95JB03736.

1271 Merle, O. and Lénat, J.F., 2003. Hybrid collapse mechanism at Piton de la Fournaise volcano,
1272 Reunion Island, Indian Ocean. *J. Geophys. Res.*, 108, 2166, doi:10.1029/2002JB002014.

1273 Michon, L. and Saint-Ange, F., 2008. Morphology of Piton de la Fournaise basaltic shield
1274 volcano (La Réunion Island): Characterization and implication in the volcano evolution. *J.*
1275 *Geophys. Res.*, 113(B3): doi:10.1029/2005JB004118.

1276 Michon, L., Saint-Ange, F., Bachèlery, P., Villeneuve, N., Staudacher, T., 2007. Role of the
1277 structural inheritance of the oceanic lithosphere in the magmato-tectonic evolution of Piton
1278 de la Fournaise volcano (La Réunion Island). *J. Geophys. Res.* 112(B4):
1279 doi:10.1029/2006JB004598.

1280 Michon, L., Di Muro, A., Villeneuve, N., Saint-Marc, C., Fadda, P., Manta, F., 2013. Explosive
1281 activity of the summit cone of Piton de la Fournaise volcano (La Réunion island): A
1282 historical and geological review. *J. Volcanol. Geotherm. Res.*, 263: 117–133,
1283 doi:10.1016/j.jvolgeores.2013.06.012.

1284 Michon, L., Ferrazzini, V., Di Muro, A., Villeneuve, N., Famin, V., 2015. Rift zones and magma
1285 plumbing system of Piton de la Fournaise volcano: How do they differ from Hawaii and
1286 Etna? *J. Volcanol. Geotherm. Res.* 303: 112–129, doi:10.1016/j.jvolgeores.2015.07.031.

1287 Miklius, A., Lisowski, M., Delaney, P.T., Denlinger, R.P., Dvorak, J.J., Okamura, A.T., and
1288 Sako, M.K., 1995. Recent inflation and flank movement of Mauna Loa volcano. In: Rhodes,

1289 J.M., Lockwood, J.P. (Eds.), *Mauna Loa Revealed: Structure, Composition, History, and*
1290 *Hazards. Am. Geophys. Un. Geophys. Mono.*, pp.199–205, doi:10.1029/GM092p0199.

1291 Miklius, A., Cervelli, P., Sako, M., Lisowski, M., Owen, S., Segall, P., Foster, J., Kamibayashi,
1292 K. and Brooks, B., 2005. *Global Positioning System Measurements on the Island of Hawai'i:*
1293 *1997 through 2004. U.S. Geol. Surv. Open-File Rep.*, 2005–1425, 46 pp.

1294 Montgomery-Brown, E.K., Segall, P. and Miklius, A., 2009. *Kilauea slow slip events:*
1295 *Identification, source inversions, and relation to seismicity. J. Geophys. Res.*, 114(B6):
1296 doi:10.1029/2008JB006074.

1297 Montgomery-Brown, E.K., Sinnett, D.K., Poland, M., Segall, P., Orr, T., Zebker, H. and Miklius,
1298 A., 2010. *Geodetic evidence for an echelon dike emplacement and concurrent slow-slip*
1299 *during the June 2007 intrusion and eruption at Kīlauea volcano, Hawaii. J. Geophys. Res.*,
1300 115(B7): doi:10.1029/2009JB006658.

1301 Montgomery-Brown, E.K., Poland, M.P. and Miklius, A., 2015. *Delicate balance of magmatic-*
1302 *tectonic interaction at Kīlauea Volcano, Hawai'i, revealed from slow slip events. In: Carey,*
1303 *R.J., Cayol, V., Poland, M.P., Weis, D. (Eds.), Hawaiian Volcanoes, From Source to Surface.*
1304 *Am. Geophys. Un. Geophys. Mono.*, 208, pp. 269–288, doi:10.1002/9781118872079.ch13.

1305 Moore, J.G., 1964. *Giant submarine landslides on the Hawaiian Ridge. U.S. Geol. Surv. Prof.*
1306 *Pap. 501-D.*, pp. D95–D98.

1307 Moore, J.G. and Krivoy, H.L., 1964. *The 1962 flank eruption of Kilauea Volcano and structure*
1308 *of the east rift zone. J. Geophys. Res.*, 69(10): 2033–2045, doi:10.1029/JZ069i010p02033.

1309 Moore, J. G., Clague, D. A., Holcomb, R. T., Lipman, P. W., Normark, W. R., Torresan, M. E.,
1310 1989. *Prodigious submarine landslides on the Hawaiian Ridge, J. Geophys. Res.* 94(B12):
1311 17,465–17,848, doi:10.1029/JB094iB12p17465.

1312 Morgan, J.K., Moore, G.F., Hills, D.J. and Leslie, S., 2000. *Overthrusting and sediment accretion*
1313 *along Kilauea's mobile south flank, Hawaii: Evidence for volcanic spreading from marine*
1314 *seismic reflection data. Geology*, 28(7): 667–670, doi:10.1130/0091-
1315 7613(2000)28<667:OASAAK>2.0.CO;2.

1316 Morgan, W.J., 1981. *Hotspot tracks and the opening of the Atlantic and Indian Oceans. In:*
1317 *Emiliani, C. (ed.), The Sea. Wiley, New York*, pp. 443–487.

1318 Münn, S., Walter, T.R., and Klügel, A., 2006. *Gravitational spreading controls rift zones and*
1319 *flank instability on El Hierro, Canary Islands. Geol. Mag.*, 143(3): 257–268,
1320 doi:10.1017/S0016756806002019.

1321 Nakamura, K., 1980, *Why do long rift zones develop in Hawaiian volcanoes: A possible role of*
1322 *thick oceanic sediments. Bull. Volcanol. Soc. Japan*, 25: 255–269 (in Japanese, with English
1323 *Abstr.*).

1324 Neri, M., Guglielmino, F., Rust, D., 2007. *Flank instability on Mount Etna: Radon, radar*
1325 *interferometry and geodetic data from the southwestern boundary of the unstable sector, J.*
1326 *Geophys. Res.*, 112(B4): doi:10.1029/2006JB004756.

1327 Norini, G. and Acocella, V., 2011. *Analogue modeling of flank instability at Mount Etna:*
1328 *understanding the driving factors. J. Geophys. Res.*, 116(B7), doi:10.1029/2011JB008216.

1329 Oehler, J.F., Labazuy, P., Lénat, J.F., 2004. *Recurrence of major flank landslides during the last*
1330 *2-Ma-history of Reunion Island. Bull. Volcanol.*, 66(7): 585–598, doi:10.1007/s00445-
1331 004-0341-2.

1332 Oehler, J.F., van Wyk de Vries, B., Labazuy, P., 2005. *Landslides and spreading of oceanic*
1333 *hotspot and arc shield volcanoes on Low Strength Layers (LSLs): An analogue modelling*
1334 *approach. J. Volcanol. Geotherm. Res.*, 144(1–4): 169–189,

1335 doi:10.1016/j.jvolgeores.2004.11.023.

1336 Oehler, J.F., Lénat, J.F., Labazuy, P., 2008. Growth and collapse of the Reunion Island
1337 volcanoes, *Bull. Volcanol.* 70(6): 717–742, doi:10.1007/s00445-007-0163-0.

1338 Orr, T.R., Poland, M.P., Patrick, M.R., Thelen, W.A., Sutton, A.J., Elias, T., Thornber, C.R.,
1339 Parcheta, C. and Wooten, K.M., 2015. Kīlauea's 5–9 March 2011 Kamoamoā fissure eruption
1340 and its relation to 30+ years of activity from Pu‘u ‘Ō ‘ō. In: Carey, R.J., Cayol, V., Poland,
1341 M.P., Weis, D. (Eds.), *Hawaiian Volcanoes, From Source to Surface*. Am. Geophys. Un.
1342 Geophys. Mono., 208, pp. 393–420, doi:10.1002/9781118872079.ch18.

1343 Owen, S., Segall, P., Freymueller, J.T., Miklius, A., Denlinger, R.P., Arnadottir, T., Sako, M.K.
1344 and Bürgmann, R., 1995. Rapid deformation of the south flank of Kilauea Volcano, Hawaii.
1345 *Science*, 267(5202): 1328–1332, doi:10.1126/science.267.5202.1328.

1346 Owen, S., Segall, P., Lisowski, M., Miklius, A., Denlinger, R. and Sako, M., 2000a. Rapid
1347 deformation of Kilauea Volcano: Global Positioning System measurements between 1990
1348 and 1996. *J. Geophys. Res.*, 105(B8): 18,983–18,993, doi:10.1029/2000JB900109.

1349 Owen, S., Segall, P., Lisowski, M., Miklius, A., Murray, M., Bevis, M. and Foster, J., 2000b.
1350 January 30, 1997 eruptive event on Kilauea Volcano, Hawaii, as monitored by continuous
1351 GPS. *Geophysical Research Letters*, 27(17): 2757–2760, doi:10.1029/1999GL008454.

1352 Patanè, D., De Gori, P., Chiarabba, C., Bonaccorso, A., 2003. Magma ascent and the
1353 pressurization of Mount Etna's volcanic system. *Science*, 299(5615), 2061–2063,
1354 doi:10.1126/science.1080653.

1355 Patanè, G., Montalto, A., Imposa, S., Menza, S., 1994. The role of regional tectonics, magma
1356 pressure and gravitational spreading in earthquakes of the eastern sector of Mt. Etna
1357 volcano (Italy). *J. Volcanol. Geotherm. Res.*, 61(3–4): 253–266, doi:10.1016/0377-
1358 0273(94)90007-8.

1359 Peltier, A., Staudacher, T., Bachèlery, P., 2007. Constraints on magma transfers and structures
1360 involved in the 2003 activity at Piton de La Fournaise from displacement data. *J. Geophys.*
1361 *Res.*, 112(B3): doi:10.1029/2006JB004379.

1362 Peltier, A., Famin, V., Bachèlery, P., Cayol, V., Fukushima, Y., Staudacher, T., 2008. Cyclic
1363 magma storages and transfers at Piton de La Fournaise volcano (La Réunion hotspot)
1364 inferred from deformation and geochemical data. *Earth Planet. Sci. Lett.* 270(3–4): 180–
1365 188, doi:10.1016/j.epsl.2008.02.042.

1366 Peltier, A., Bachèlery, P., Staudacher, T., 2009. Magma transfer and storage at Piton de La
1367 Fournaise (La Réunion Island) between 1972 and 2007: A review of geophysical and
1368 geochemical data. *J. Volcanol. Geotherm. Res.* 184(1–2), 93–108,
1369 doi:10.1016/j.jvolgeores.2008.12.008.

1370 Peltier, A., Massin, F., Bachèlery, P., Finizola, A., 2012. Internal structures and building of
1371 basaltic shield volcanoes: The example of the Piton de La Fournaise terminal cone (La
1372 Réunion). *Bull. Volcanol.* 74(8): 1881–1897, doi:10.1007/s0044501206367.

1373 Peltier, A., Poland, M.P., Staudacher, T., 2015a. Are Piton de la Fournaise (La Réunion) and
1374 Kīlauea (Hawai‘i) Really “Analog Volcanoes. In: Carey, R.J., Cayol, V., Poland, M.P.,
1375 Weis, D. (Eds.), *Hawaiian Volcanoes, From Source to Surface*. Am. Geophys. Un.
1376 Geophys. Mono., 208, pp. 507–531, doi:10.1002/9781118872079.ch23.

1377 Peltier, A., Got, J.-L., Villeneuve, N., Boissier, P., Staudacher, T., Ferrazzini, V., Walpersdorf,
1378 A., 2015b. Long-term mass transfer at Piton de la Fournaise volcano evidenced by strain
1379 distribution derived from GNSS network. *J. Geophys. Res.*, 120(3): 1874–1889,
1380 doi:10.1002/2014JB011738.

1381 Peltier, A., Beauducel, F., Villeneuve, N., Ferrazzini, V., Di Muro, A., Aiuppa, A., Derrien, A.,
1382 Jourde, K., Taisne, B., 2016. Deep fluid transfer evidenced by surface deformation during
1383 the 2014–2015 unrest at Piton de la Fournaise volcano. *J. Volcanol. Geotherm. Res.*, 321:
1384 140–148, doi :10.1016 :j.jvolgeores.2016.04.031.

1385 Phillips, K.A., Chadwell, C.D. and Hildebrand, J.A., 2008. Vertical deformation measurements
1386 on the submerged south flank of Kilauea volcano, Hawai'i reveal seafloor motion associated
1387 with volcanic collapse. *J. Geophys. Res.*, 113(5): doi:10.1029/2007JB005124.

1388 Plattner, C., Amelung, F., Baker, S., Govers, R. and Poland, M.P., 2013. The role of viscous
1389 magma mush spreading in volcanic flank motion at Kīlauea Volcano, Hawai'i. *J. Geophys.*
1390 *Res.*, 118(5): 2474–2487, doi:10.1002/jgrb.50194.

1391 Poland, M.P., 2014a. Contrasting Volcanism in Hawai'i and the Galápagos. In: Harpp, K.S.,
1392 Mittelstaedt, E., d'Ozouville, N., Graham, D.W. (Eds.), *The Galápagos: A Natural*
1393 *Laboratory for the Earth Sciences. Am. Geophys. Un. Geophys. Mono.*, 204, pp. 5–26,
1394 doi:10.1002/9781118852538.ch2.

1395 Poland, M.P., 2014b. Time-averaged discharge rate of subaerial lava at Kīlauea Volcano,
1396 Hawai'i, measured from TanDEM-X interferometry: Implications for magma supply and
1397 storage during 2011–2013. *J. Geophys. Res.*, 119(7): 5464–5481,
1398 doi:10.1002/2014JB011132.

1399 Poland, M.P., Miklius, A., Orr, T., Sutton, A.J., Thornber, C.R. and Wilson, D., 2008. New
1400 episodes of volcanism at Kilauea Volcano, Hawaii. *EOS Trans. Am. Geophys. Un.*, 89(5):
1401 37–38, doi:10.1029/2008EO050001.

1402 Poland, M.P., Miklius, A., Sutton, A.J. and Thornber, C.R., 2012. A mantle-driven surge in
1403 magma supply to Kilauea Volcano during 2003–2007. *Nature Geosci.*, 5(4): 295–300,
1404 doi:10.1038/ngeo1426.

1405 Poland, M.P., Miklius, A. and Montgomery-Brown, E.K., 2014. Magma supply, storage, and
1406 transport at shield-stage Hawaiian volcanoes. In: Poland, M.P., Landowski, C.M., Takahashi,
1407 T.J. (Eds.), *Characteristics of Hawaiian Volcanoes. U.S. Geol. Surv. Prof. Pap.*, 1801, pp.
1408 179–234, doi:10.3133/pp18015.

1409 Prôno, E., Battaglia, J., Monteiller, V., Got, J.-L., Ferrazzini, V., 2009. P-wave velocity structure
1410 of Piton de la Fournaise volcano deduced from seismic data recorded between 1996 and
1411 1999. *J. Volcanol. Geotherm. Res.* 184(1–2): 49–62, doi:10.1016/j.jvolgeores.2008.12.009.

1412 Puglisi, G., Bonforte, A., Maueri, S.R., 2001. Ground deformation patterns on Mt. Etna, 1992
1413 to 1994, inferred from GPS data. *Bull. Volcanol.*, 62(6): 371–384
1414 doi:10.1007/s004450000112.

1415 Puglisi, G., Bonforte, A., Ferretti, A., Guglielmino, F., Palano, M., Prati, C., 2008. Dynamics of
1416 Mount Etna before, during, and after the July–August 2001 eruption inferred from GPS
1417 and differential synthetic aperture radar interferometry data. *J. Geophys. Res.*, 113(B6):
1418 doi:10.1029/2006JB004811.

1419 Robinson, J.E. and Eakins, B.W., 2006. Calculated volumes of individual shield volcanoes at the
1420 young end of the Hawaiian Ridge. *J. Volcanol. Geotherm. Res.*, 151(1–3): 309–317,
1421 doi:10.1016/j.jvolgeores.2005.07.033.

1422 Roult, G., Peltier, A., Taisne, B., Staudacher, T., Ferrazzini, V., Di Muro, A., the OVPF team,
1423 2012. A new comprehensive classification of the Piton de la Fournaise activity spanning
1424 the 1985–2010 period: Search and analysis of short-term precursors from a broad-band
1425 seismological station. *J. Volcanol. Geotherm. Res.*, 241–242: 78–104,
1426 doi:10.1016/j.jvolgeores.2012.06.012.

- 1427 Ruch, J., Acocella, V., Storti, F., Neri, M., Pepe, S., Solaro, G., Sansosti, E., 2010. Detachment
1428 depth revealed by rollover deformation: An integrated approach at Mount Etna. *Geophys.*
1429 *Res. Lett.*, 37, L16304, doi:10.1029/2010GL044131.
- 1430 Ruch, J., Pepe, S., Casu, F., Acocella, V., Neri, M., Solaro, G., Sansosti, E., 2012. How do
1431 volcanic rift zones relate to flank instability? Evidence from collapsing rifts at Etna.
1432 *Geophys. Res. Lett.*, 39, L20311, doi:10.1029/2012GL053683.
- 1433 Ruch, J., Pepe, S., Casu, F., Solaro, G., Pepe, A., Acocella, V., Neri, M., Sansosti, E., 2013.
1434 Seismo-tectonic behavior of the Pernicana Fault System (Mt Etna): A gauge for volcano
1435 flank instability? *J. Geophys. Res.*, 118(8): 4398–4409, doi:10.1002/jgrb.50281.
- 1436 Rust, D. and Neri, M., 1996. The boundaries of large-scale collapse on the flanks of Mount Etna,
1437 Sicily. In: McGuire, W.J., Jones, A.P., Neuberg, J. (Eds.), *Volcano Instability on the Earth*
1438 *and Other Planets. Geol. Soc. Spec. Publ.*, 110, pp. 193–208.
- 1439 Saint-Ange, F., Bachèlery, P., Babonneau, N., Michon, L., Jorry, S.J., 2013. Volcaniclastic
1440 sedimentation on the submarine slopes of a basaltic hotspot volcano: Piton de la Fournaise
1441 volcano (La Réunion Island, Indian Ocean). *Marine Geol.* 337: 35–52,
1442 doi:10.1016/j.margeo.2013.01.004.
- 1443 Schaefer, L.N., Lu, Z. and Oommen, T., 2015. Dramatic volcanic instability revealed by InSAR.
1444 *Geology*, 43(8): 743–746, doi:10.1130/G36678.1.
- 1445 Schaefer, L., Lu, Z. and Oommen, T., 2016. Post-Eruption Deformation Processes Measured
1446 Using ALOS-1 and UAVSAR InSAR at Pacaya Volcano, Guatemala. *Remote Sensing*, 8(1):
1447 73, doi:10.3390/rs8010073.
- 1448 Schmincke, H.-U., 1982. Volcanic and chemical evolution of the Canary Islands. In: von Rad,
1449 U., Hinz, K., Sarnthein, M., Seibold, E. (Eds.), *Geology of the Northwest African*
1450 *Continental Margin*, pp. 273–301, doi:10.1007/978-3-642-68409-8_12.
- 1451 Segall, P., Desmarais, E.K., Shelly, D., Miklius, A. and Cervelli, P., 2006. Earthquakes triggered
1452 by silent slip events on Kilauea volcano, Hawaii. *Nature*, 442(7098): 71–74,
1453 doi:10.1038/nature04938.
- 1454 Shirzaei, M., Bürgmann, R., Foster, J., Walter, T.R. and Brooks, B.A., 2013. Aseismic
1455 deformation across the Hilina fault system, Hawaii, revealed by wavelet analysis of InSAR
1456 and GPS time series. *Earth Planet. Sci. Lett.*, 376: 12–19, doi:10.1016/j.epsl.2013.06.011.
- 1457 Siniscalchi, A., Tripaldi, S., Neri, M., Balasco, M., Romano, G., Ruch, J., Schiavone, D., 2012.
1458 Flank instability structure of Mt. Etna inferred by a magnetotelluric survey. *J. Geophys.*
1459 *Res.*, 117(3): doi: 10.1029/2011JB008657.
- 1460 Solaro, G., Acocella, V., Pepe, S., Ruch, J., Neri, M., Sansosti E., 2010. Anatomy of an unstable
1461 volcano from InSAR: Multiple processes affecting flank instability at Mt. Etna, 1994–
1462 2008. *J. Geophys. Res.*, 115(B10): doi:10.1029/2009JB000820.
- 1463 Staudacher, T., Peltier, A., 2016. Ground deformation at Piton de la Fournaise (La Réunion
1464 Island), a review from 20 years of GNSS monitoring. In: Bachèlery, P., Lénat, J.F., Di
1465 Muro, A., Michon, L. (Eds.), *Active volcanoes of the Southwest Indian Ocean: Piton de la*
1466 *Fournaise and Karthala*, pp. 139–170, doi:10.1007/978-3-642-31395-0_9.
- 1467 Swanson, D.A., Duffield, W.A. and Fiske, R.S., 1976. Displacement of the south flank of
1468 Kilauea Volcano: the result of forceful intrusion of magma into the rift zones. *U.S. Geol.*
1469 *Surv. Prof. Pap.*, 963, 39 pp.
- 1470 Swanson, D.A., Rose, T.R., Mucek, A.E., Garcia, M.O., Fiske, R.S. and Mastin, L.G., 2014.
1471 Cycles of explosive and effusive eruptions at Kīlauea Volcano, Hawai‘i. *Geology*, 42(7):
1472 631–634, doi:10.1130/G35701.1.

1473 Swanson, D.A., Fiske, R.S., Thornber, C.R., and Poland, M.P., in preparation. Dikes in the
1474 Koa‘e fault system, and the Koa‘e-east rift zone structural grain at Kīlauea Volcano, Hawai‘i.
1475 Intended for Geol. Soc. Am. Sp. Pap.

1476 Tibaldi, A., 2001. Multiple sector collapses at Stromboli volcano, Italy: How they work. *Bull.*
1477 *Volcanol.*, 63(2): 112–125, doi: 10.1007/s004450100129.

1478 Tibaldi, A., Groppelli, G., 2002. Volcano-tectonic activity along structures of the unstable NE
1479 flank of Mt. Etna (Italy) and their possible origin. *J. Volcanol. Geotherm. Res.*, 115(3–4):
1480 277–302, doi: 10.1016/S0377-0273(01)00305-5..

1481 Tilling, R.I. and Dvorak, J.J., 1993. Anatomy of a basaltic volcano. *Nature*, 363(6425): 125–133,
1482 doi:10.1038/363125a0.

1483 Tinard, P., 2007. Caractérisation et modélisation des déplacements du sol associés à l'activité
1484 volcanique du Piton de la Fournaise, île de La Réunion, à partir de données
1485 interférométriques. Août 2003 – Avril 2007. PhD Thesis, Université de Clermont Ferrand,
1486 334 pp.

1487 Tridon, M., Cayol, V., Forger, J.L., Augier, A., Bachèlery, P., 2016, Inversion of coeval shear
1488 and normal stress of Piton de la Fournaise flank displacement. *J. Geophys. Res.*, 121(11):
1489 7846–7866, doi:10.1002/2016JB013330.

1490 Urgeles, R., Canals, M., Baraza, J., Alonso, B., Masson, D., 1997. The most recent
1491 megalandslides of the Canary Islands: El Golfo debris avalanche and Canary debris flow,
1492 west El Hierro Island. *J. Geophys. Res.*, 102(B9): 20,305–20,323, doi:10.1029/97JB00649.

1493 Van Ark, E. and Lin, J., 2004. Time variation in igneous volume flux of the Hawaii-Emperor hot
1494 spot seamount chain. *J. Geophys. Res.*, 109(B11): doi:10.1029/2003JB002949.

1495 van Wyk de Vries, B. and Borgia, A., 1996. The role of basement in volcano deformation. In:
1496 McGuire, W.J., Jones, A.P., Newberg, J. (Eds.), *Volcano Instability on the Earth and Other*
1497 *Planets*. Geol. Soc. Lon. Sp. Pub., 110, pp. 95–110.

1498 Villeneuve, N., Bachèlery, P., 2006. Revue de la typologie des éruptions au Piton de La
1499 Fournaise, processus et risques volcaniques associés. *Cybergeo: Eur. J. Geogr.*,
1500 doi:10.4000/cybergeo.2536.

1501 Villeneuve, N., Bachèlery, P., Kemp, J., 2014. La Réunion Island: A typical example of a
1502 basaltic shield volcano with rapid evolution. In: Fort, M., André, M.-F. (Eds.), *Landscapes*
1503 *and Landforms of France*, pp. 261–270, doi:10.1007/978-94-007-7022-5_25.

1504 Walter, T.R., Troll, V.R., Cailleau, B., Belousov, A., Schmincke, H.U., Amelung, F. and
1505 Bogaard, P.v.d., 2005. Rift zone reorganization through flank instability in ocean island
1506 volcanoes: an example from Tenerife, Canary Islands. *Bull. Volcanol.*, 67(4): 281–291,
1507 doi:10.1007/s00445-004-0352-z.

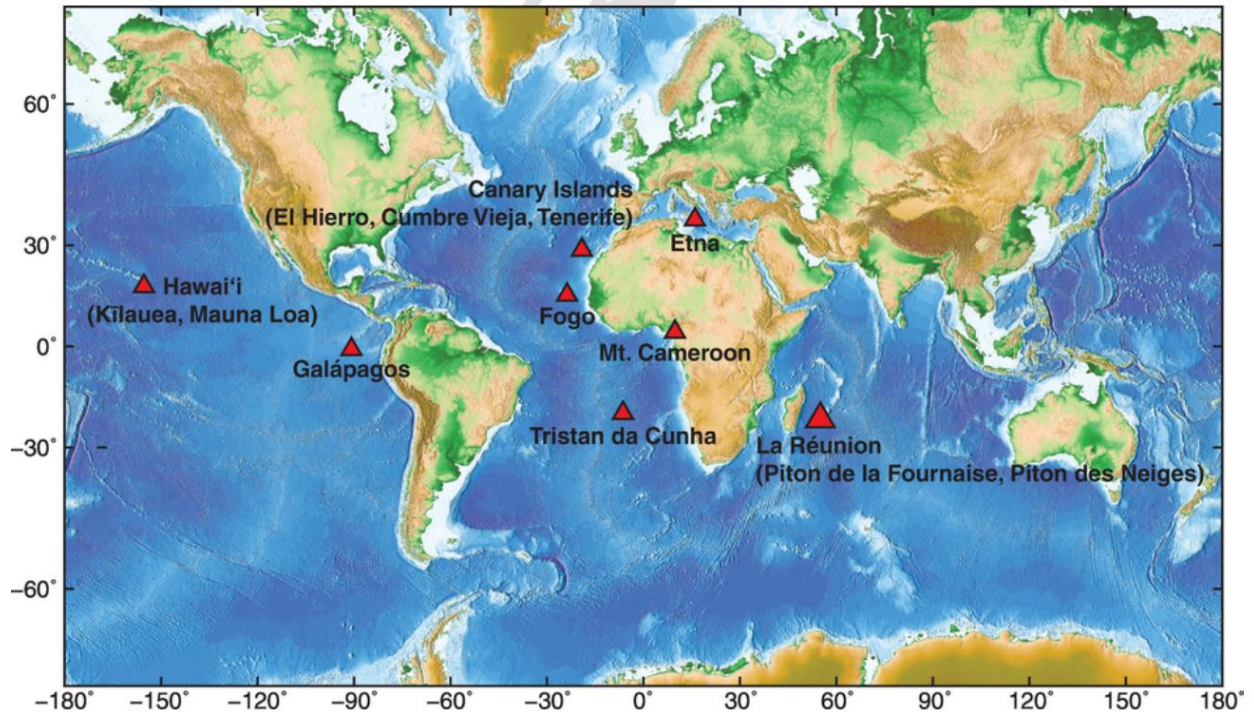
1508 White, R. S., 1993. Melt production rates in mantle plumes. *Philos. Trans. R. Soc. Lond. Ser. A*,
1509 342(1663): 137–153, doi:10.1098/rsta.1993.0010.

1510 Wolfe, C.J., Brooks, B.A., Foster, J.H. and Okubo, P.G., 2007. Microearthquake streaks and
1511 seismicity triggered by slow earthquakes on the mobile south flank of Kilauea Volcano,
1512 Hawai‘i. *Geophys. Res. Lett.*, 34(23): doi:10.1029/2007GL031625.

1513 Wright, T.L. and Klein, F.W., 2014. Two hundred years of magma transport and storage at
1514 Kilauea Volcano, Hawai‘i, 1790–2008. *U.S. Geol. Surv. Prof. Pap.*, 1806,
1515 doi:10.3133/pp1806.

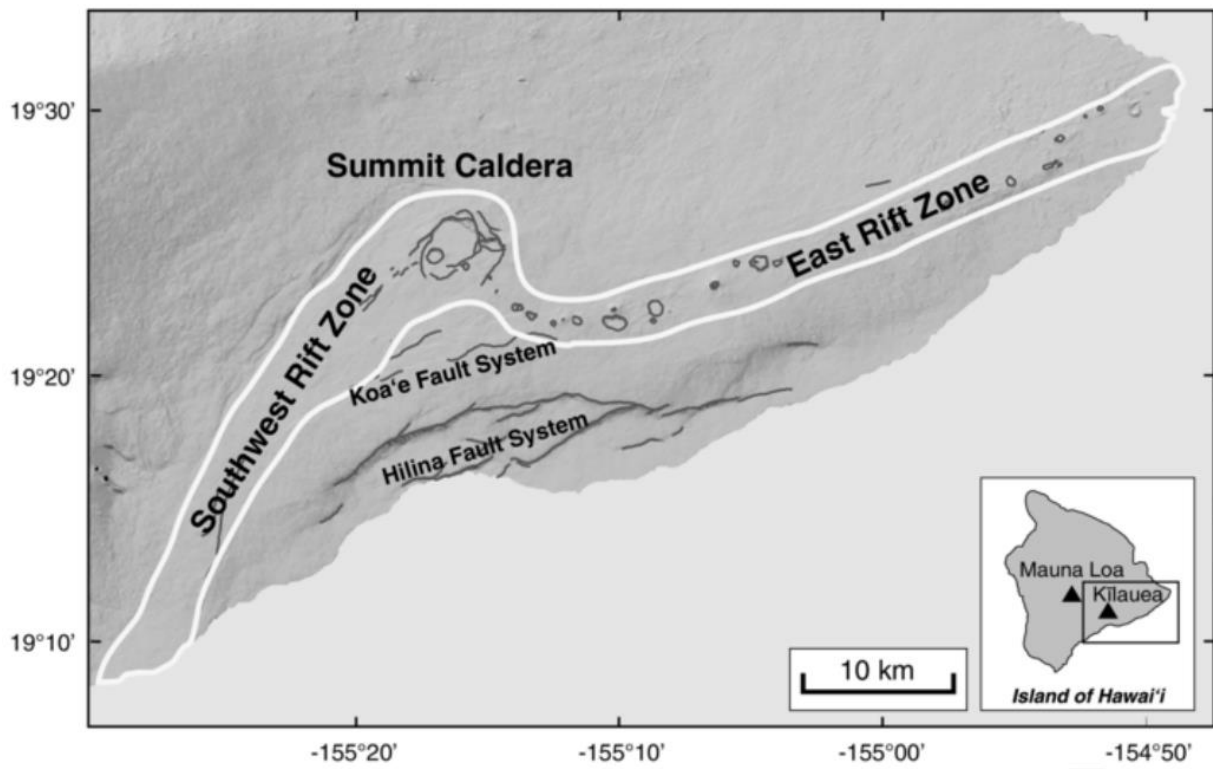
1516
1517

1518



1519
1520
1521

Figure 1



1522
1523
1524
1525

Figure 2

1526

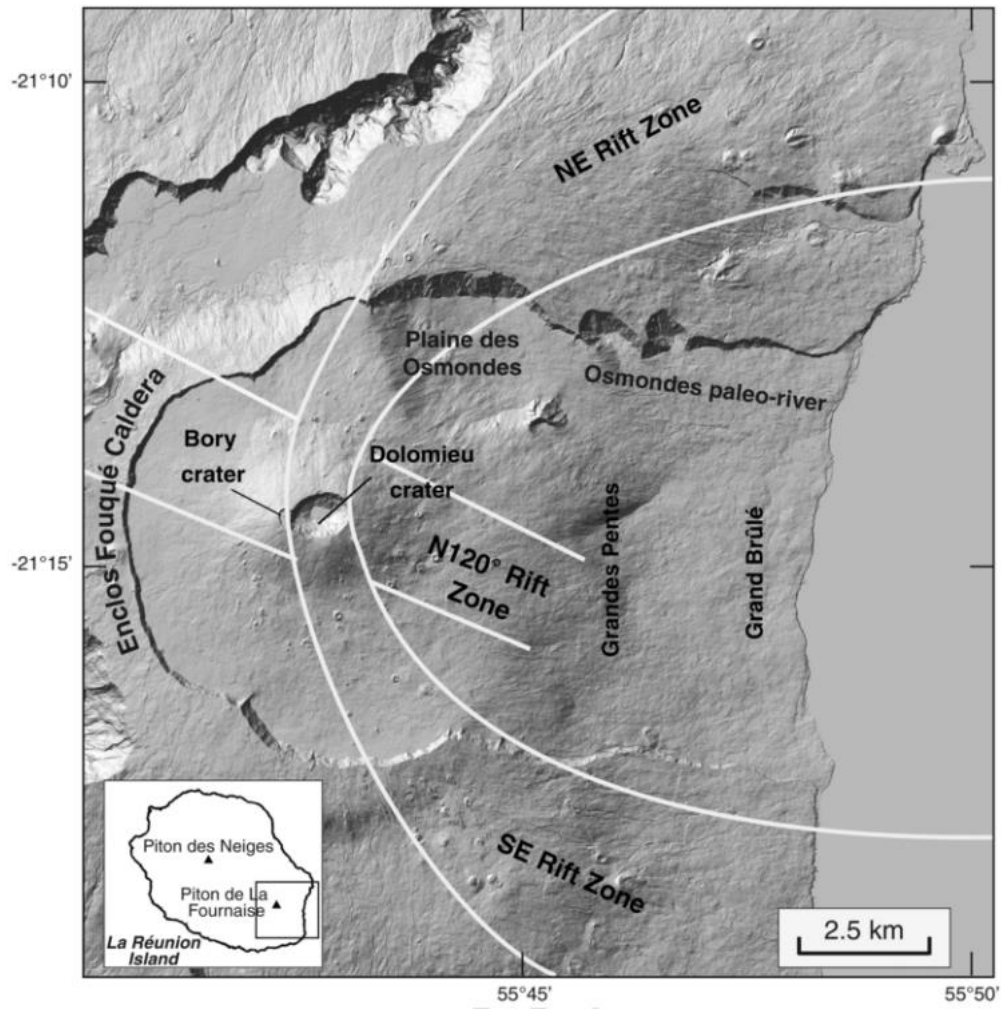


Figure 3

1527
1528
1529
1530

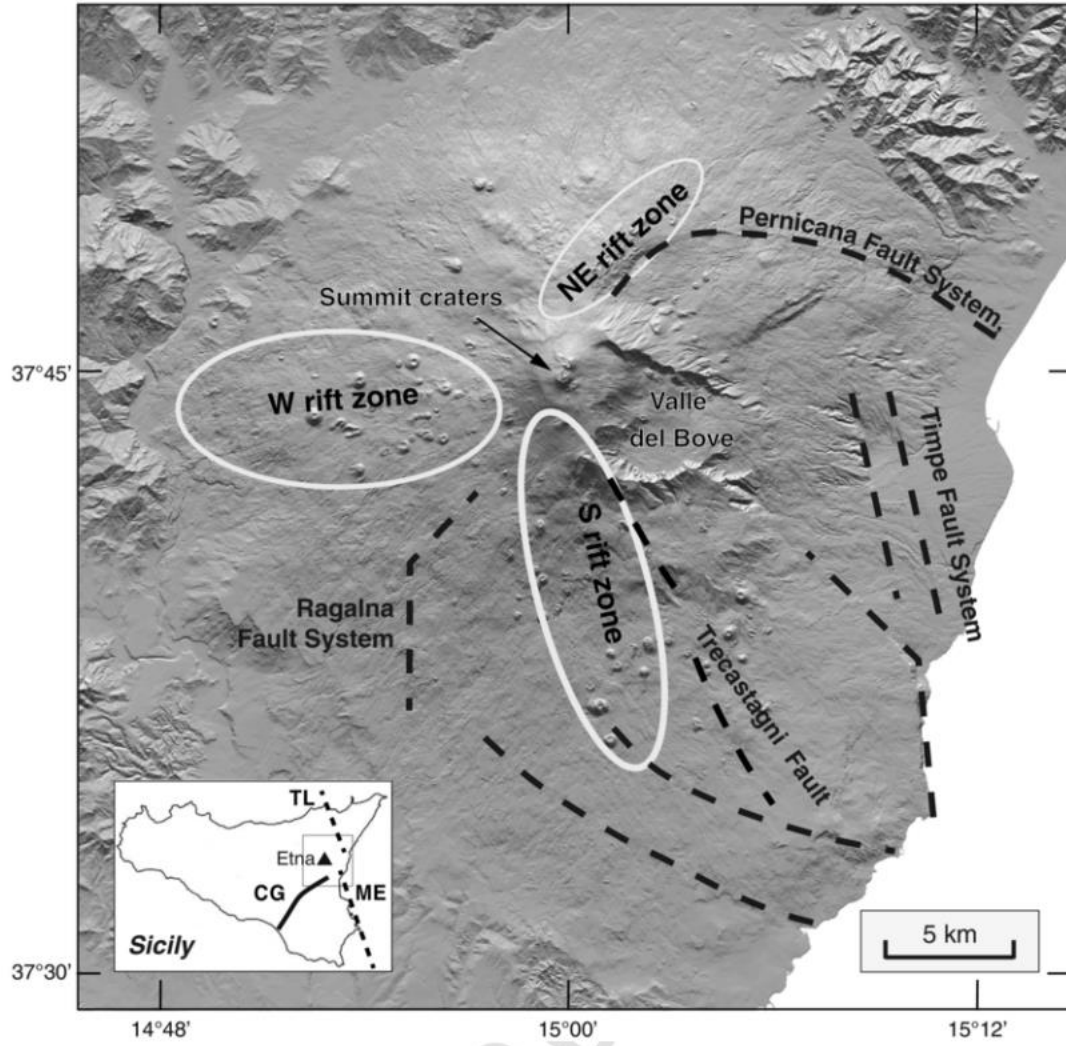
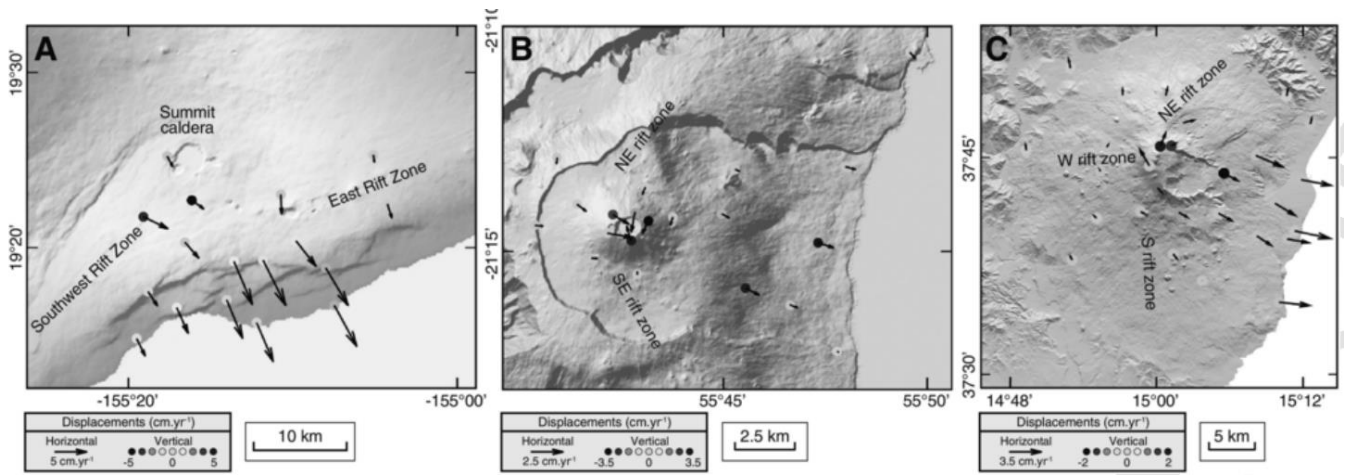


Figure 4

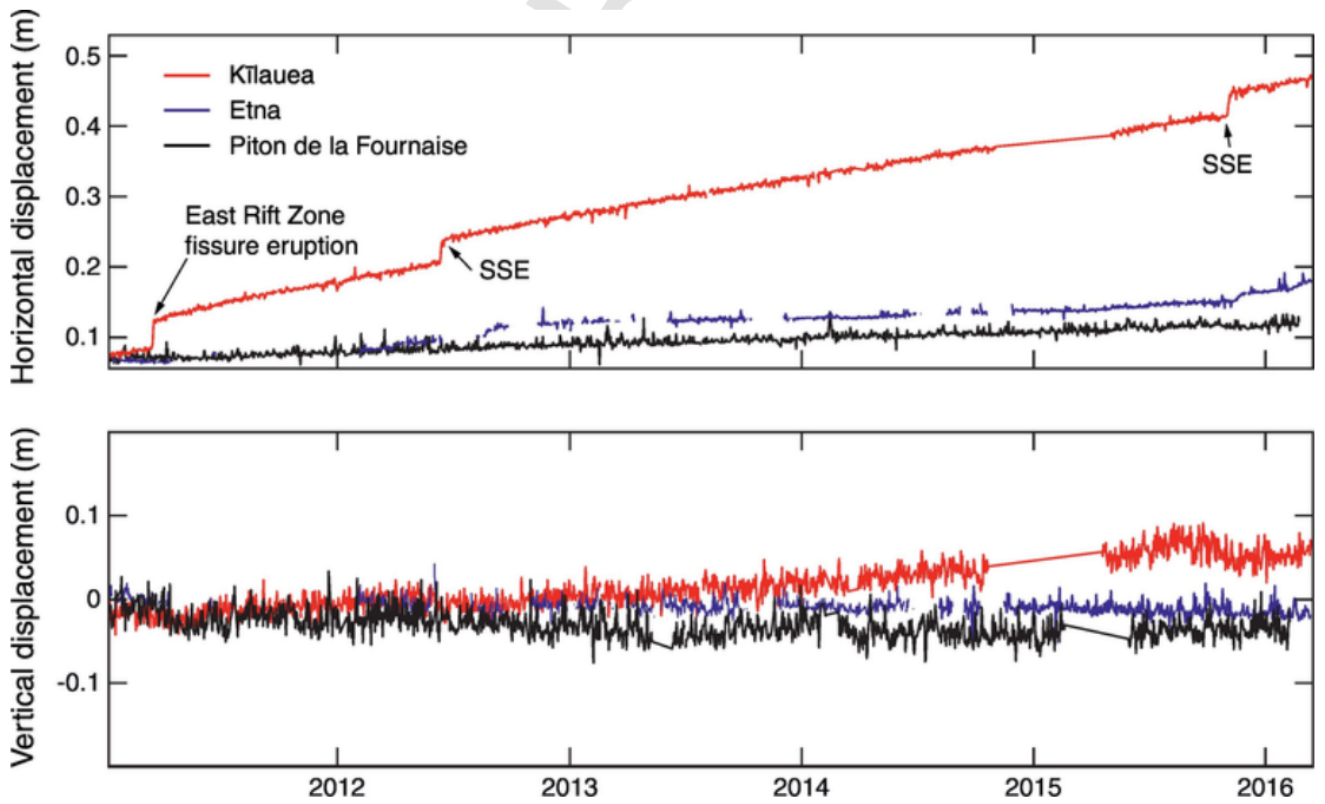
1531
 1532
 1533
 1534

1535



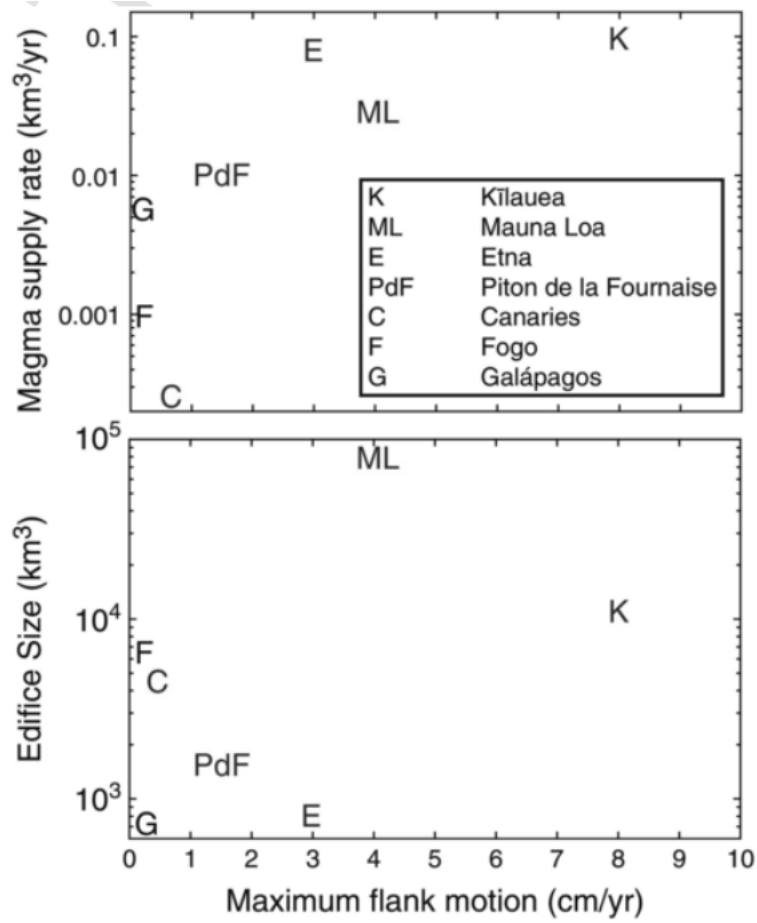
1536
1537
1538
1539

Figure 5



1540
1541
1542
1543

Figure 6



1544
 1545
 1546
 1547

Figure 7

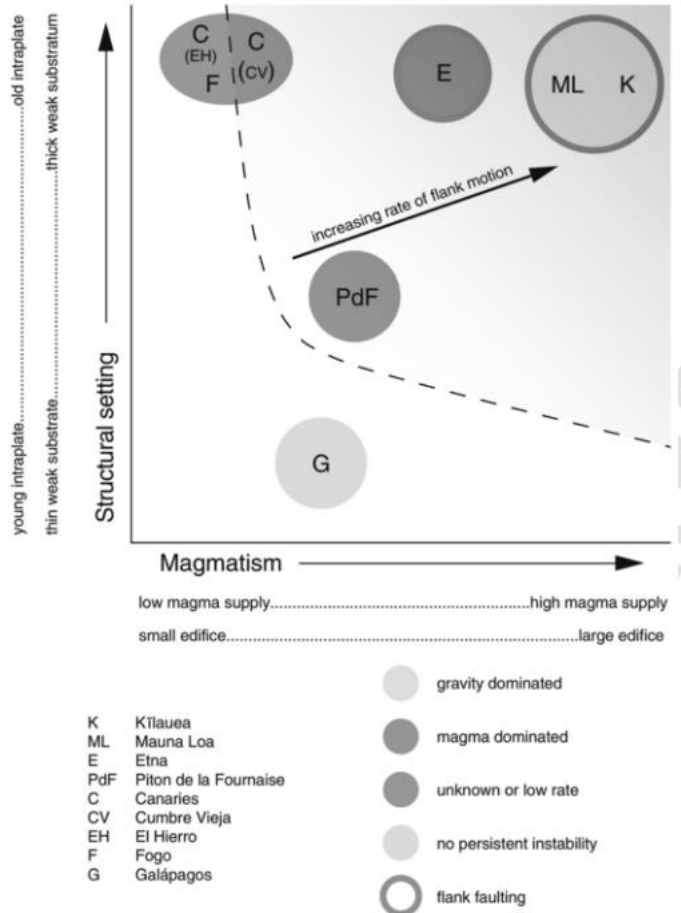


Figure 8

1548
1549
1550